Struct Bond (2007) 123: 41–78
DOI 10.1007/430_037

Published online: 22 July 2006

From Photoinduced Charge Separation to Light-driven Molecular Machines

Etienne Baranoff[1] · Francesco Barigelletti[2] · Sylvestre Bonnet[1] · Jean-Paul Collin[1] · Lucia Flamigni[2] · Pierre Mobian[1] · Jean-Pierre Sauvage[1] (✉)

[1]Laboratoire de Chimie Organo-Minérale, UMR 7513 du CNRS, Institut Le Bel, Université Louis Pasteur, 4 rue Blaise Pascal, 67000 Strasbourg Cedex, France
sauvage@chimie.u-strasbg.fr

[2]Istituto ISOF-CNR, Via P. Gobetti 101, 40129 Bologna, Italy

Abstract The photochemical properties of transition metal complexes, such as those of iridium(III) or ruthenium(II), can be exploited in various ways to generate charge-separated (CS) states, in relation to the mimicry of the natural photosynthetic reaction centres, or to set multicomponent compounds or assemblies in motion. The first part of the present chapter summarizes the work carried out in our groups (Bologna and Strasbourg) in recent years with iridium(III)-terpy complexes (terpy: 2,2′,6′,6″-terpyridine). The synthesis of multicomponent iridium(III) complexes in reasonable yields has been

achieved and their photochemical properties have been investigated. Unexpectedly, the excited state lifetimes of some of these compounds are very long at room temperature (several microseconds) in fluid solution, making the $Ir(terpy)_2^{3+}$ fragment an interesting chromophore. Once attached to electron donor (D) groups, dyads of the $Ir(terpy)_2^{3+}$-D type undergo fast photoinduced electron transfer. In addition $Ir(terpy)_2^{3+}$ in the ground state is a relatively good electron acceptor, displaying interesting properties as electron relay in porphyrinic triads. A triad, consisting of an $Ir(terpy)_2^{3+}$ central core, a Zn porphyrin as the primary donor on one side and a gold(III) porphyrin as the terminal acceptor on the other side, leads to a relatively long-lived CS state (close to the microsecond). The other section of the present chapter deals with light-driven molecular machines built around $Ru(bpy)_3^{2+}$ derivatives, including catenanes and rotaxanes. In order to set the system in motion, a dissociative ligand field (LF) state is generated from the light-absorbing metal-to-ligand charge transfer (MLCT) state, originating in the expulsion of a given ligand and in a perfectly controlled fashion. This step is rapidly followed by coordination of another ligand to afford a kinetically stable new complex. The process can be inverted by thermal energy, so as to regenerate the starting state of the system.

Keywords Catenane · Ir/Ru · Light-driven molecular machine · Photoinduced Charge Separation · Rotaxane · Scorpionate

Abbreviations

A	Acceptor
bpqpy	2,6-bis(4′-phenyl-2′-quinolyl)-pyridine
bpy	2,2′-bipyridine
CR	Charge Recombination
CS	Charge Separation or Charge Separated
CT	Charge Transfer
D	Donor
dmbp	6,6′-dimethyl-2,2′-bipyridine
dmp	2,9-dimethyl-1,10-phenanthroline
DPAA	di-*p*-anisylamine
dpbp	6,6′-diphenyl-2,2′bipyridine
DQ	*N*,*N*′-polymethylene bridged-2,2′-bipyridinium
HOMO	Highest Occupied Molecular Orbital
ILCT	Intra Ligand Charge Tranfer
LC	Ligand Centered
LF	Ligand Field
LLCT	Ligand to Ligand Charge Transfer
LUMO	Lowest Unoccupied Molecular Orbital
MLCT	Metal to Ligand Charge Transfer
MV	1,1′-dimethyl-4,4′-bipyridinium, methyl viologen
OLED	Organic Light-Emitting Diode
PC	Photoactive Centre
phen	1,10-phenanthroline
PTZ	phenothiazine
py	pyridine
RCM	Ring Closing Metathesis
terpy	2,2′ : 6′,2″-terpyridine
tterpy	4′-(*p*-tolyl)-2,2′ : 6′,2″-terpyridine

1 Introduction

Several decades ago, inorganic photochemistry was mostly devoted to the photochemical reactivity of transition metal complexes: by shining light onto a transition metal complex, one or several photoproducts were obtained and analyzed. In this respect, inorganic photochemistry could be considered as an interesting *synthetic* method [1, 2].

The seventies have seen the triumph of $Ru(bpy)_3^{2+}$ and its numerous congeners, in relation to solar energy conversion [3, 4]. Gradually, the excited state became, in the photochemists' mind, a powerful energy or electron transfer agent instead of a molecular species to be converted to another one.

Many multicomponent transition metal complexes have been elaborated in the course of the last 15 to 20 years, with the aim of inducing charge separation under the action of light, so as to generate reasonably long-lived charge separated (CS) states. The first part of this review article relates to this active field of research.

One of the favourite generic arrangement is the molecular triad, consisting of a photoactive centre (PC), an electron donor (D) and an electron acceptor (A). In systems such as D-PC-A, the charge separated state D^+-PC-A^- is obtained in two consecutive-electron transfer processes after excitation of PC. Of course, several variants exist, depending on the electron transfer properties of PC and its excited state, PC*, as well as on the precise arrangement of the various components (PC-A_1-A_2 or D_2-D_1-PC, in particular, if PC* is an electron donor or an electron acceptor, respectively).

Ir(III) complexes containing terpy type ligands (terpy = 2,2′ : 6′,2″-terpyridine) have been shown to behave as strong electron acceptors in their excited state and as interesting electron relays in their ground state. These unusual properties, distinctly different from those of their Ru(II) analogues, have been exploited to construct molecular dyads and triads incorporating $Ir(terpy)_2^{3+}$ fragments.

The field of dynamic molecular systems, for which given parts of the compounds or assemblies can be set in motion in a highly controlled fashion, is most of the time referred to as "molecular machines". This new field of research seems to attract much interest from organic chemistry and coordination chemistry teams. Most of the molecular machines containing transition metal centres are driven using electrochemistry (reduction or oxidation of the metal centre). An alternative approach, reviewed in the second part of the present chapter, is based on photochemistry. The excited state is now considered, again, as a photoreagent whose function will be more complex than just exchanging energy or an electron. A real photochemical reaction will take place (expulsion of a ligand if light excitation generates a dissociative excited state), which will be at the origin of a large amplitude motion. Another stimulus will have to invert the motion and regenerate the starting state

of the complex. In this respect, this very recent aspect of the molecular machine area goes back to the previous work mentioned at the beginning of the introduction, dealing with preparative photochemistry. The main difference holds in the complexity of the ligand backbones now utilized to construct the molecular machines in question.

2 Charge Separation on Derivatives of $Ir(terpy)_2^{3+}$ Used as Electron Relay or Photoactive Centre

We will review here work wherein several types of species incorporate the Ir-bis-terpy unit and derivatives. The search for multicomponent arrays, including metal-based photoactive centres in combination with electron donor and acceptor components, was started a couple of decades ago, and one of the first systems, compound $\mathbf{1}^{4+}$, was studied by Meyer et al. (Fig. 1) [5]. In this multicomponent system, the electron donor phenothiazine (PTZ) and the bridged 2,2′-bipyridinium (DQ) units are linked to the photoactive unit by flexible methylene connections. In this early example, excitation at the Ru-based chromophore ultimately yields a PTZ^+-DQ^- CS state which lives 165 ns and for which the transiently stored energy is 1.29 eV.

We will see how our work extended such types of studies and gradually led to several types of Ru(II)- and Os(II)-based dyadic and triadic species and how the Ir(III)-bis-terpy-based photosensitizers emerged as convenient units to build up linearly arranged multicomponent arrays. It should be mentioned here that Ir(III)-cyclometalated complexes, both of bidentate and tridentate ligands, have proved to be convenient for use as singlet oxygen sensitizers [6, 7], as biological labelling reagents [8] and as efficient phosphors in

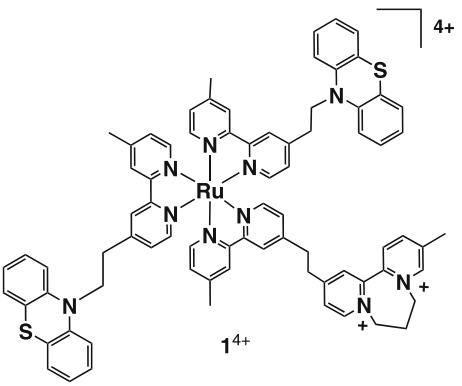

Fig. 1 Chemical structure of compound $\mathbf{1}^{4+}$

the area of OLED fabrication [9–16]. For the last type of application, the research activity is expanding remarkably and several uncharged (neutral) Ir(III) species are being tested as phosphorescent dopant within these electroluminescent devices. The neutral character is a basic requirement to avoid the physical displacement of these luminophores upon application of the electric field to generate the electron and hole flux within the device. Ir(III) compounds featuring exceptionally high luminescent quantum yields (not far from unity) [9, 13] and tunable emission colours [14, 17–19] have been characterised and their incorporation within various types of OLEDs looks very promising. However, we shall restrict ourselves to applications aimed at the study of the photoinduced charge separation. For these, Ir-bis-terpyridine derivatives prove to be the basic unit of choice.

2.1
Early Work on Systems Based on Ru(II) and Os(II) bis-Terpyridine Complexes

Compounds $\mathbf{2}^{4+}$–$\mathbf{5}^{4+}$ (Fig. 2) were the first systems studied by our groups with the aim of achieving charge separation over a nanometric array [20, 21]. The arrays are based on Ru(II) or Os(II) bis-terpyridine decorated with a methyl viologen (MV) electron acceptor and either a di-*p*-anisylamine (DPAA) or a phenothiazine (PTZ) as electron donors; the centre-to-centre separation between the terminal units can be evaluated to be ca. 1.7 nm. In comparison to other systems based on bidentate ligands [5], these structures have the advantage of a rigid, linear geometry well suited for the construction of wire-type arrays, without the possibility of different isomers. Excitation of the metal

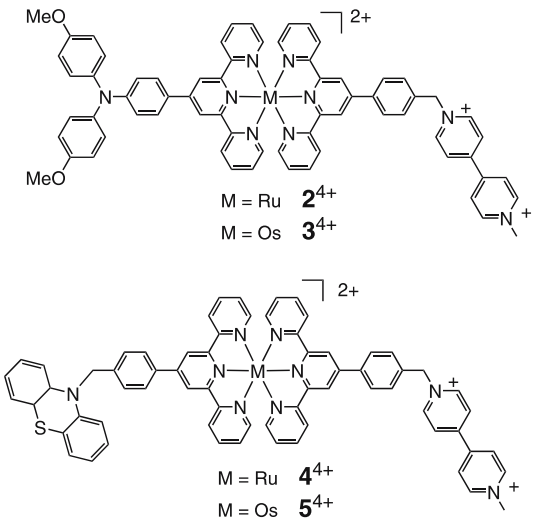

Fig. 2 Chemical structures of compounds $\mathbf{2}^{4+}$, $\mathbf{3}^{4+}$, $\mathbf{4}^{4+}$ and $\mathbf{5}^{4+}$

complex unit leads to population of the metal to ligand charge transfer triplet excited state (^{3}MLCT) displaying lifetimes of 0.95 ns and 230 ns at room temperature for the complexes, Ru(tterpy)$_2^{2+}$, and Os(tterpy)$_2^{2+}$ respectively. Due to the short lifetime of the former at room temperature, the determinations in the triads were performed in fluid solutions at low temperature (155 K) to increase the lifetime of the excited state. For comparison purposes the triads based on Os(tterpy)$_2^{2+}$, in addition to room temperature, were also studied at 155 K.

For the Ru-based DPAA-Ru-MV triad, the photoinduced processes are summarized in Scheme 1. In this approximate scheme, the excited state energy levels are derived from the luminescence data (λ_{max} at 77 K), and the energy of the charge separated states are derived from the redox potentials by simple addition of the energy necessary to oxidize the donor and the energy necessary to reduce the acceptor. The excitation of the Ru-based photosensitizer leads to a quenched luminescence lifetime of 15 ns as in the corresponding Ru-MV dyad which, compared to a lifetime of 800 ns for the model complex at 155 K [20], yields an electron transfer rate constant of 6.6×10^7 s^{-1}. The transient spectrum obtained in the triad after excitation of the Ru complex consists of the DPAA$^+$ radical cation band, which is formed with a lifetime of 18 ns. Therefore after formation of the primary CS state, DPAA-Ru$^+$-MV$^-$, the fully CS state, DPAA$^+$-Ru-MV$^-$, is formed and subsequently decays with a lifetime of 27 ns.

For the Os-based triad, the primary electron transfer quenching process leading to DPAA-Os$^+$-MV$^-$ takes place with $k = 6.7 \times 10^8$ s^{-1} ($\tau = 1.5$ ns), Scheme 2. As can be seen from the energy level scheme, electron transfer

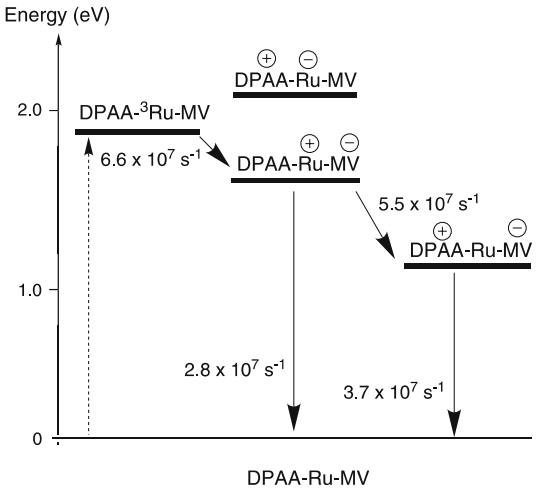

Scheme 1 Energy level diagram and reaction rates for the photoinduced processes occurring in triad $\mathbf{2}^{4+}$ at 155 K. Excitation (*dashed arrow*) on the DPAA chromophore

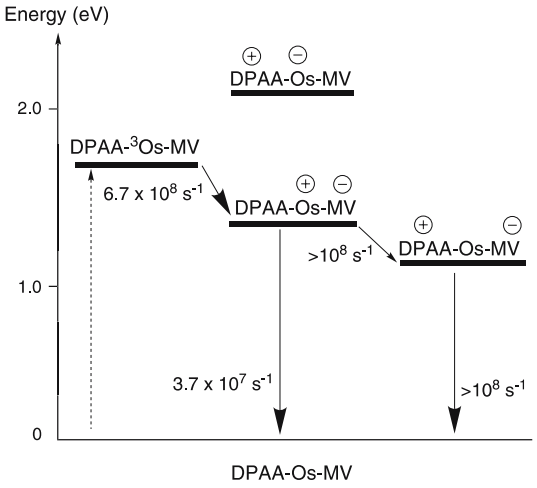

Scheme 2 Energy level diagram and reaction rates for the photoinduced processes occurring in $\mathbf{3}^{4+}$ at 155 K. Excitation (*dashed arrow*) on the DPAA chromophore

from the donor to the oxidized photosensitizer is thermodynamically feasible. Since neither $DPAA^+$ nor Os^+ absorption bands are detected in the transient spectra, it can be concluded that (i) the deactivation of DPAA-Os^+-MV^- via $DPAA^+$-Os-MV^- is faster than the rate of back electron transfer in the dyad Os-MV ($k = 3.7 \times 10^7\ s^{-1}$) and that (ii) the subsequent CR of the fully CS state $DPAA^+$-Os-MV^- is faster than the experimental resolution (ca. 10 ns), placing for the last two reactions a lower limit of $10^8\ s^{-1}$. When PTZ is used as electron donor, the system displays chemical and photochemical instability [21].

In view of the higher energy content of the ^{3}MLCT level of $Ru(tterpy)_2^{2+}$ with respect to that of $Os(tterpy)_2^{2+}$ (see Sect. 2.2), the former complex was preferred as a component for the subsequent development of the project, which involved the preparation of porphyrin-based dyads and triads. In this case both the ruthenium centre and the appended units can be excited in the visible region of the spectra. The synthetic strategy made use of the metal to act as a gathering centre for porphyrins, which were respectively either a zinc(II) porphyrin or a free-base porphyrin as donor groups (PZn or PH_2) and a gold(III) porphyrin as acceptor unit (PAu). Whereas the gold porphyrin electron acceptor unit was a tetraphenyl porphyrin in all examined cases, the early attempts made use as an electron donor of the *ethio* zinc (II)- or free-base porphyrin, $\mathbf{6}^{3+}$ and $\mathbf{7}^{3+}$ (Fig. 3) [22].

Upon excitation of the metal complex centre, triplet energy transfer to the donor appended porphyrin rapidly quenches the excited state of the central ruthenium bis-terpyridyl unit, whereas excitation of the gold porphyrin, leads in less than 1 ps to the triplet-excited state [23], which is unreactive to-

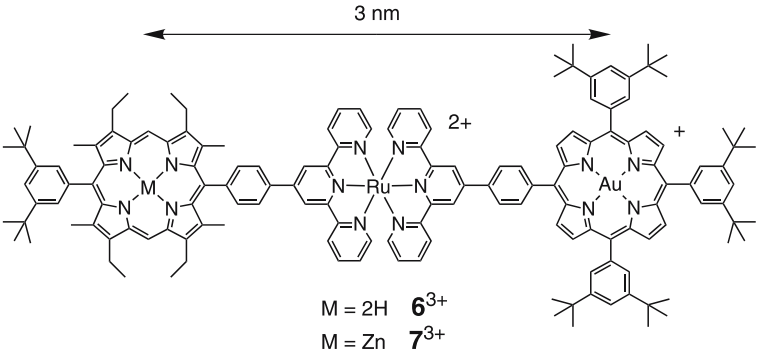

Fig. 3 Chemical structures of compounds $\mathbf{6}^{3+}$ and $\mathbf{7}^{3+}$

ward electron or energy transfer processes. These experimental results have been explained as follows [22]. Excitation into the free base moiety of $\mathbf{6}^{3+}$ produces the corresponding excited singlet state $^1PH_2 - Ru - PAu$, which transfers an electron to the adjacent Ru-based unit, forming the charge separated state $PH_2^+ - Ru^- - PAu$. The two energy levels, Scheme 3, are very close, and consequently charge transfer is expected to be highly reversible. Competing processes for the deactivation of $PH_2^+ - Ru^- - PAu$ will be: (i) back electron transfer leading directly to the ground state and (ii) further electron transfer to yield the fully CS state, $PH_2^+ - Ru - PAu^-$. This process occurs with a rate constant of $5.6 \times 10^8\ s^{-1}$ at room temperature and the CS state exhibits a lifetime of

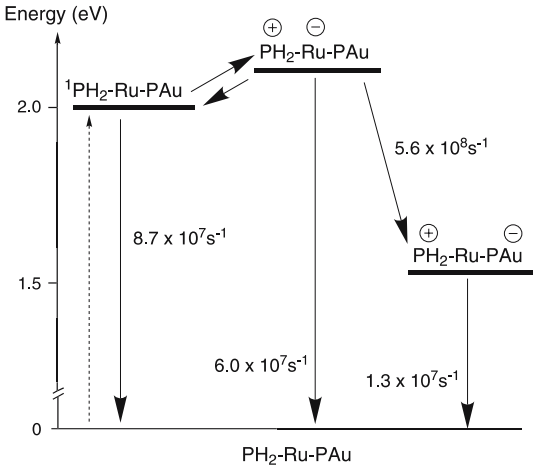

Scheme 3 Energy level diagram and reaction rates for the photoinduced processes occurring in compound $\mathbf{6}^{3+}$. The *dashed arrow* indicates excitation of the free-base porphyrin unit

75 ns in acetonitrile. On the basis of the rates reported on Scheme 3 a quantum yield of formation of charge separation (Φ_{cs}) of 0.27 can be calculated.

The triad $\mathbf{7}^{3+}$ containing the corresponding zinc porphyrin as a donor has a rather different energy level distribution (Scheme 4). Zinc porphyrin is, in fact, characterised by a higher energy level excited state (by ca. 0.1 eV) and a lower oxidation potential than the free-base counterpart by ca. 0.15–0.2 V [22]. The situation is favourable to the occurrence of electron transfer from the excited state localized on the zinc porphyrin unit, ^{1}PZn – Ru – PAu, to the ruthenium centre to form the CS state $PZn^+ – Ru^- – PAu$, and subsequently the fully CS state $PZn^+ – Ru – PAu^-$. The latter has a lifetime of 33 ns and an overall yield of charge separation $\phi_{cs} = 0.60$. The shorter lifetime with respect to the free-base counterpart was explained by the fact that the charge recombination is not occurring so deep in the Marcus inverted region ($\Delta G^0 = -1.23$ eV), as for the free-base porphyrin-containing triad ($\Delta G^0 = -1.4$ eV).

In the subsequent development of the project, the *ethio*-type porphyrin was substituted by the more robust tetraaryl porphyrin, which could better stand the drastic conditions of the synthesis [24]. This has consequences also in the energy level diagram of the systems since the presence of meso-tetraaryl groups increases by ca. 0.05–0.1 V the oxidation potential of the porphyrin compared to the *ethio* derivatives with alkyl substitution on the tetrapyrrole, and decreases the excited state energy level by ca. 0.05–0.1 eV. In general, this means that in the meso-tetraaryl-based arrays there is a decrease of the driving force for charge separation and an increase in the driving force for charge recombination with rather important effects on the photoinduced processes.

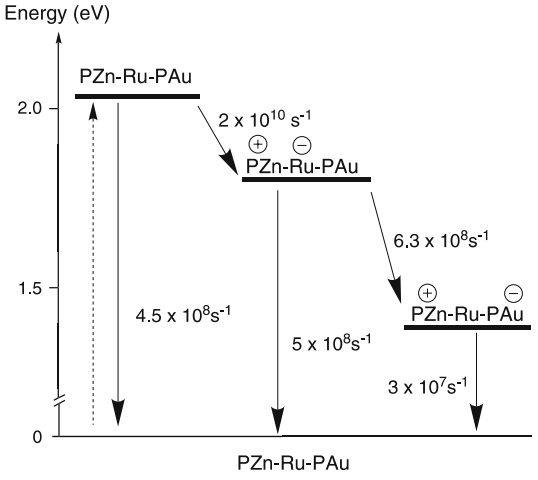

Scheme 4 Energy level diagram and reaction rates for the photoinduced processes occurring in compound $\mathbf{7}^{3+}$. The *dashed arrow* indicates excitation of the Zn porphyrin unit

Another attempt that was tried in order to improve the performances of the arrays was the introduction of some change on the structure of the central $Ru(terpy)_2^{2+}$, which could result in an increase of the lifetime of the complex at room temperature, while still maintaining the favourable geometry of the terpy ligand [25]. We reasoned that a longer lifetime of the excited metal complex unit would have allowed its use as a photosensitizer, in addition to its use as an electron relay, thus increasing the efficiency of CS upon excitation in the visible range at room temperature. To this aim a tridentate 2,6-bis(4′-phenyl-2′-quinolyl)pyridine (bpqpy) was employed as ligand, $\mathbf{8}^{2+}$ (Fig. 4) [25]. The use of this ligand with extended conjugation was expected to decrease the energy of the luminescent ^{3}MLCT excited state, thus making more difficult its deactivation via the upper lying ^{3}MC excited state (of d→d origin and whose energy gap is governed by the ligand field strength [4]), and so increasing its lifetime [26]. The energy of the excited state of $\mathbf{8}^{2+}$ was actually lower than that of $Ru(terpy)_2^{2+}$, 1.83 eV vs. 1.97 eV respectively, and also the electrochemical properties were favourable, its reduction potential ($E_{1/2}$ = – 0.83 V vs SCE) being less negative than that of $Ru(terpy)_2^{2+}$ ($E_{1/2}$ = – 1.18 eV vs SCE) [22, 25]. Unfortunately, for $Ru(terpy)(bpqpy)^{2+}$ steric crowding of the bpqpy ligand weakens the ligand field strength, resulting in an extremely short lifetime for the ^{3}MLCT state, 90 ps compared to 0.95 ns of the $Ru(terpy)_2^{2+}$. This leads to poor performances of this complex as a photosensitizer in the porphyrin dyads $\mathbf{9}^{2+}$ and $\mathbf{10}^{2+}$ (Fig. 4), in that its lifetime is too short to participate in the photoinduced

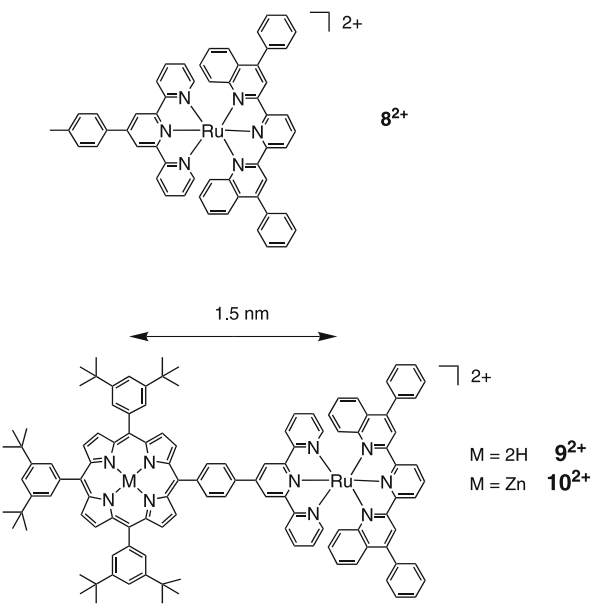

Fig. 4 Chemical structures of compounds $\mathbf{8}^{2+}$, $\mathbf{9}^{2+}$ and $\mathbf{10}^{2+}$

processes [25]. On the contrary, excitation of the porphyrin counterparts at room temperature led to charge separation, with an electron transferred from the excited state of the porphyrin to the ruthenium unit *and* energy transfer to the ^{3}MLCT excited state localized on the complex. The energy transfer process is formally spin forbidden, and is made possible by the spin-orbit coupling induced by the heavy Ru(II) centre. From the results of the photoexcitation of these systems, summarized for $\mathbf{9}^{2+}$ in Scheme 5, we started to be aware of the possible occurrence of spin-forbidden energy transfer processes, which could efficiently compete with the desired electron transfer process whenever a low-lying excited state localized on the metal complex is present [26].

The confirmation of the importance of energy transfer processes in the Ru(terpy)$_2^{2+}$-based triads came from the study of system $\mathbf{11}^{3+}$ (Fig. 5) [24].

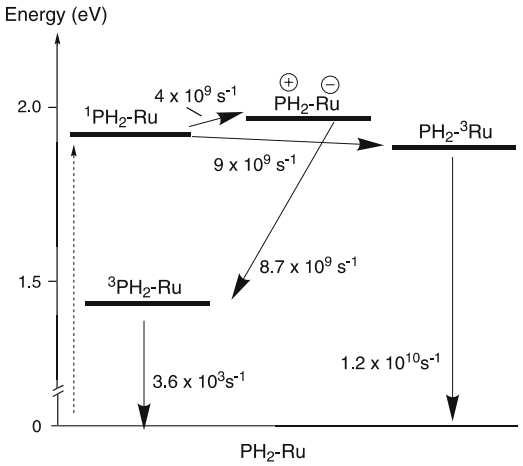

Scheme 5 Energy level diagram and reaction rates for the photoinduced processes occurring in compound $\mathbf{9}^{2+}$. The *dashed arrow* indicates excitation of the free-base porphyrin unit

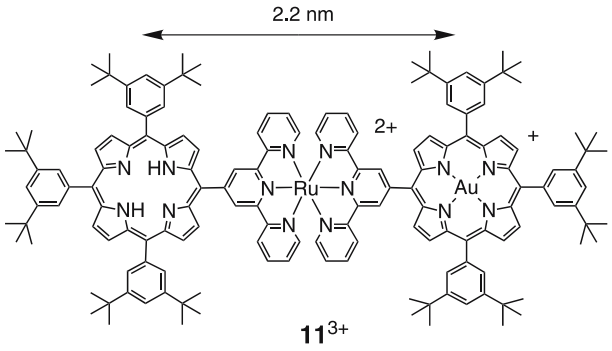

$\mathbf{11}^{3+}$

Fig. 5 Chemical structure of compound $\mathbf{11}^{3+}$

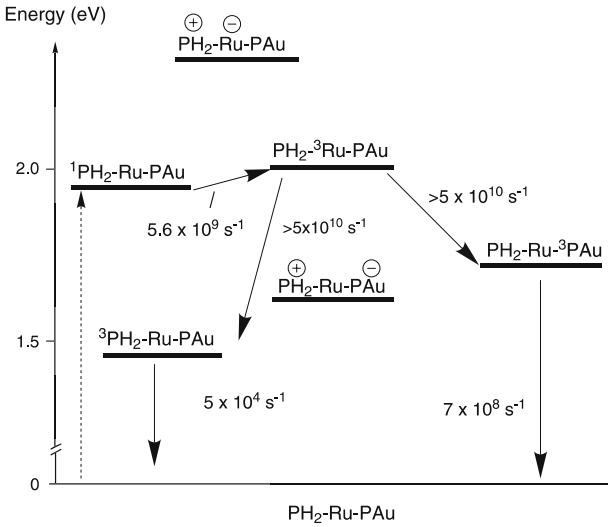

Scheme 6 Energy level diagram and reaction rates for the photoinduced processes occurring in compound $\mathbf{11}^{3+}$. The *dashed arrow* indicates excitation of the free-base porphyrin unit

The energy level diagram of this system is reported in Scheme 6; the charge separated state with the oxidized porphyrin and the reduced ruthenium complex is high in energy and electron transfer from excited porphyrin to the metal complex unit cannot take place. The only thermodynamically feasible electron transfer reaction following excitation of porphyrin would be direct transfer of an electron to the gold porphyrin unit, but in spite of the coupling of the components in this array, with the phenyl spacer missing between the components, electron transfer across the metal complex does not occur. The experimental data in $\mathbf{11}^{3+}$ were explained as follows, see Scheme 6 [24].

After excitation into the free base porphyrin moiety, leading to $^1PH_2 - Ru - PAu$, an initial energy transfer occurs to the triplet state of the central metal complex, $PH_2 - {}^3Ru - PAu$ with a slightly endoergonic process. This state deactivates rapidly ($k > 5 \times 10^{10}\ s^{-1}$) through two energy transfer pathways to either the triplet state of the free base, $^3PH_2 - Ru - PAu$, or to the triplet state localized on the gold porphyrin, $PH_2 - Ru - {}^3PAu$. From the experimental ratio of the porphyrin triplet yields, $\Phi^3_{PAu}/\Phi^3_{PH_2}$, the relative efficiencies of the energy transfer steps are estimated to be 4 in favour of the gold porphyrin triplet. The lifetime of the triplet localized on the gold porphyrin is the same as in the model PAu, $\tau = 1.4$ ns, indicating that this state is inactive toward energy or electron transfer processes. The triplet lifetime of the free base porphyrin is slightly reduced with $\tau = 20\ \mu s$ compared to the model PH_2, very likely for the effect of heavy ruthenium ion on the intersystem crossing rate [24]. At 77 K in glassy solvent, the lifetime of the gold porphyrin triplet

increases to 90 μs, and in this condition it can transfer energy to the lower energy triplet state localized on the free base $^3PH_2 - Ru - PAu$, which becomes the final recipient of the light energy absorbed by the system [27].

The results here presented for the systems $\mathbf{9}^{2+}$, $\mathbf{10}^{2+}$ and $\mathbf{11}^{3+}$, have clearly pointed out that the presence of a metal complex component with a low-lying excited state (≤ 2.0 eV) can be detrimental to the efficiency of electron transfer.

2.2 $Ir(terpy)_2^{3+}$ and Derivatives: Photophysical Properties

The complexes of the Ir(III)-, Ru(II)-, and Os(II)- bis-terpy type have the nearly planar terpyridine systems perpendicularly arranged to each other. On this basis, a convenient linear arrangement for dyads and triads can be obtained by designing species having opposite groups appended at the 4′ position of the two ligands, see Sect. 2.1; examples of Ru(II) and Os(II) cases are complexes $\mathbf{2}^{4+}$, $\mathbf{3}^{4+}$, $\mathbf{4}^{4+}$ and $\mathbf{5}^{4+}$. This contrasts favourably with what happens with related complexes containing three bidentate ligands like bpy or phen, for example complex $\mathbf{1}^{4+}$ and derived molecular assemblies [5, 28]. Actually, Ru(II)- and Os(II)-tris-bpy (or phen) complexes exhibit good luminescence properties, both in terms of luminescence efficiency and lifetimes [4, 29]; however, the appended groups at the ligands give rise to dyads and triads that cannot exhibit a linear geometry [5, 30]; in addition, the presence of stereoisomers results in mixtures of species. In fact, only one case has been reported wherein the use of bidentate ligands might be amenable to the construction of the sought for linear arrangement of multicentre species; this occurs when a helical bis-phen ligand (which actually behaves as a tetradentate ligand) is coordinated to a Ru(II) centre, $\mathbf{12}^{2+}$ (Fig. 6) [31].

Unfortunately, most Ru(II)-bis-terpy type complexes are poor luminophores [26], even if several preparative approaches have afforded species with

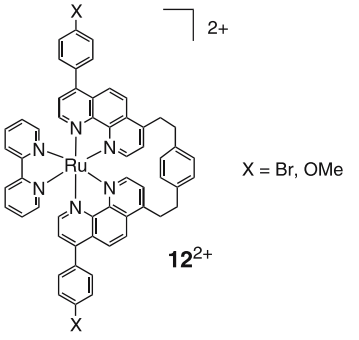

Fig. 6 Chemical structure of compounds $\mathbf{12}^{2+}$

Table 1 Photophysical parameters of Ir(III) tris-bpy and bis-terpy complexes; properties for related complexes of Ru(II) and Os(II) are also listed [a]

	λ_{abs} (nm) [b] (ε, M^{-1} cm^{-1})	λ_{em} (nm) [c]	ϕ_{em} [d]	τ [d] (μs)	E_{0-0} (eV) [e]	Emitting state	Refs.
$Ir(bpy)_3^{3+}$ [f]	344 (3300)	441	–	[2.4]	2.81		[32, 33]
$Ir(terpy)_2^{3+}$ ($\mathbf{13}^{3+}$) [f]	352 (5800)	458	2.5×10^{-2}	1.0 [1.2]	2.71	LC	[34]
$\mathbf{14}^{3+}$ [f]	372 (13200)	506	2.6×10^{-2}	2.3		LC/MLCT	[34]
$Ir(tterpy)_2^{3+}$ ($\mathbf{15}^{3+}$) [f]	373 (29000)	506	2.9×10^{-2}	2.4 [9.5]	2.45	LC/MLCT	[34]
$\mathbf{16}^{3+}$	372 (23800)	506	2.2×10^{-2} [9.3×10^{-2}])	1.6 [6.8])	2.55	LC/MLCT	[34] [35]
$\mathbf{17}^{3+}$	380 (27000)	570	0.21×10^{-2} [0.55×10^{-2}]	0.49 [0.80]	2.43		[35]
$\mathbf{18}^{3+}$	398 (45000)	566	0.27×10^{-2} [0.76×10^{-2}]	0.58 [2.0]	2.41		[35]
$\mathbf{19}^{3+}$	377 (29200)	550	0.2×10^{-2}	0.73	2.4	MLCT	[36]
$\mathbf{20}^{3+}$	321 (53300), 504 (44800)	754 [g]	[h]	[h]	[h]	ILCT [g]	[17]
$\mathbf{21}^{3+}$	321 (50600), 493 (35100)	784 [g]	[h]	[h]	[h]	ILCT [g]	[17]
$\mathbf{22}^{3+}$	322 (31700), 476 (9400)	[h]	[h]	[h]	[h]	[h]	[17]
$Ru(bpy)_3^{2+}$	451 (13000)	610	1.5×10^{-2} [6.2×10^{-2}]	0.17 [0.90]	2.03	MLCT	[4, 37, 38]
$Ru(terpy)_2^{2+}$ [f]	474 (14600)	~ 630	$< 5 \times 10^{-5}$	250 ps	2.07	MLCT	[39]
$Ru(tterpy)_2^{2+}$	490 (28000)	640	3.2×10^{-5}	0.95 ns	1.98	MLCT	[26]
$Os(bpy)_3^{2+}$		718	3.2×10^{-3} [5×10^{-3}]	49 ns 60 ns	1.75	MLCT	[29, 38]
$Os(terpy)_2^{2+}$	477 (13800), 657 (3700)	718	1.2×10^{-3} [1.4×10^{-2}]	0.03 [0.27]	1.8	MLCT	Our results and [26]
$Os(tterpy)_2^{2+}$	490 (26000), 667 (6600)	734	2.3×10^{-3} [2.1×10^{-2}]	0.02 [0.22]	~ 1.8	MLCT	Our results and [26]

[a] Room temperature, in air-equilibrated acetonitrile unless otherwise indicated, PF_6^- salts
[b] Lowest energy band(s) with $\varepsilon > 1000$
[c] Highest energy peak maximum
[d] In *square brackets*, values in degassed solvent
[e] Energy content of the luminescent level estimated from fits of the luminescence profile at room temperature or from the luminescence band maximum at 77 K
[f] Alcoholic solvent
[g] The emission properties undergo changes in protic solvent
[h] Not determined

significantly enhanced luminescence properties [40–43]. As for the Os(II)-bis-terpy complexes, these exhibit convenient luminescence properties, but the luminescent level can only store a low energy content, ~ 1.8 eV, Table 1. A comparison of spectroscopic properties for representative iridium bis-terpyridine complexes, reported in Fig. 7, and related ruthenium and osmium complexes is provided in this table. Several iridium bis-terpyridine complexes are strongly luminescent at room temperature ($\phi_{em} \sim 10^{-2}$), with lifetimes on the microseconds time scale. Importantly, the energy content of the emission level is high, in several cases larger than 2.5 eV, which contrasts favourably with that of the Ru(II) and Os(II) based counterparts, ca. 2 and 1.8 eV, respectively. For the Ir(III) complexes, the nature of the excited states responsible

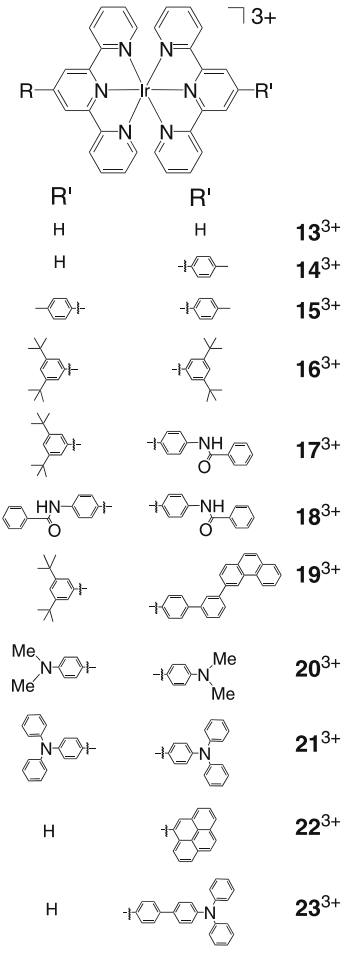

Fig. 7 Chemical structures of compounds **13**$^{3+}$ to **23**$^{3+}$

for luminescence may vary from LC to MLCT and to ILCT depending on the electronic properties of the groups appended at the 4,4′-positions of the terpy ligands (Table 1). In some cases, the luminescence due to the Ir-bis-terpy unit appears substantially quenched, as it happens for the series of complexes $\mathbf{20}^{3+}$–$\mathbf{23}^{3+}$ (Fig. 7) [17]. This is due to the presence of low-lying levels, a consequence of the nature of the appended groups; for instance, the electron-donating properties of amino-benzene units may result in scarcely emitting low-lying levels of ILCT nature, cases of $\mathbf{20}^{3+}$, $\mathbf{21}^{3+}$, and $\mathbf{23}^{3+}$ [17]. Nevertheless, the remarkable luminescence properties and the high energy content of the luminescent level for most of the Ir(III) bis-terpy complexes, in combination with their geometric properties, make them very attractive candidates as photosensitizers in dyadic and triadic schemes. In addition, their ease of reduction ($E_{1/2}$ ca. – 0.75 V vs. SCE) compared to Os(II) and Ru(II) complexes, ($E_{1/2}$ ca. – 1.2 V vs. SCE) makes them very promising electron acceptor or electron relay units in dyadic and triadic schemes for charge separation [26, 34].

2.3
Ir as Electron Relay: The Molecular Triads PH_2-Ir(III)-PAu^{4+} and PZn-Ir(III)-PAu^{4+}

Having verified that the photophysical and electrochemical properties of the $Ir(terpy)_2^{3+}$ derivatives were satisfying the characteristics we looked for, in that the excited state energy was well above 2 eV and that reduction was easier than for the related $Ru(terpy)_2^{2+}$ derivatives, we decided to use $Ir(terpy)_2^{3+}$ as assembling unit and as electron relay in the following evolution of the project. We then synthesized two triads based on the Ir(III) complex, using zinc or free base tetra-aryl-porphyrin as the donor and photoactive centre and a gold tetraarylporphyrin as the acceptor.

The energy level diagram for the triad containing the free base, $\mathbf{24}^{4+}$ (Fig. 8), is reported in Scheme 7 [44, 45].

Excitation of the free base porphyrin unit in $\mathbf{24}^{4+}$ leads to the excited state $^1PH_2 - Ir - PAu$, which is quenched to a lifetime of 30 ps, compared to

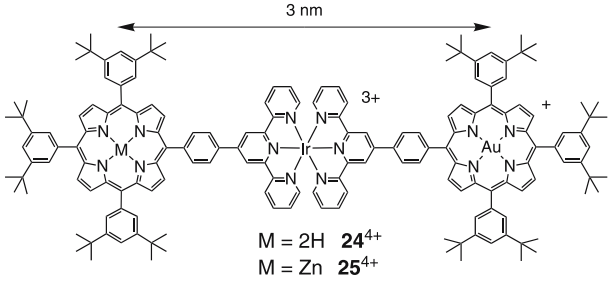

Fig. 8 Chemical structures of compounds $\mathbf{24}^{4+}$ and $\mathbf{25}^{4+}$

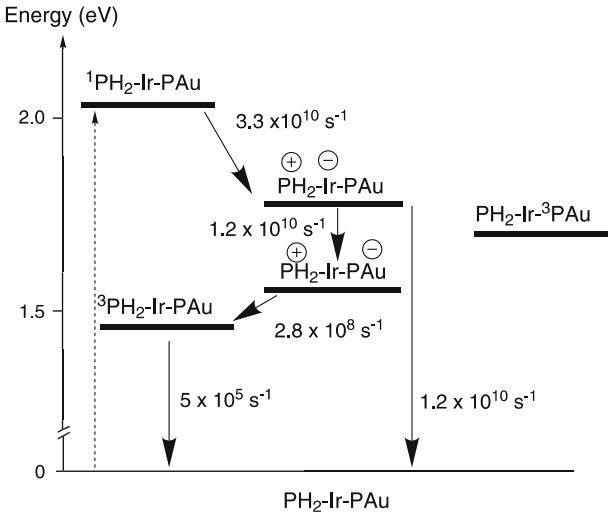

Scheme 7 Energy level diagram and reaction rates for the photoinduced processes occurring in compound $\mathbf{24}^{4+}$. The *dashed arrow* indicates excitation of the free-base porphyrin unit

a lifetime of 8.3 ns for the model porphyrin. The quenching does not occur in butyronitrile glass at 77 K, where the lifetime of the singlet is 11 ns, the same as that of the model. Deactivation can be assigned to an electron transfer from the singlet state localized on the free base $^1PH_2 - Ir - PAu$ to the central Ir complex core to yield the charge separated state $PH_2^+ - Ir^- - PAu$, the electron being localized on a terpy ligand. On the other hand, excitation of the PAu part leads rapidly to the triplet state of the gold porphyrin $PH_2 - Ir - {}^3PAu$, which decays with a lifetime of 1.4 ns as the model porphyrin, indicating that this state is not photoactive, as previously noticed. Deactivation of the primary CS state is faster in the triad (40 ps) than in the model $PH_2 - Ir$ dyad (75 ps), indicating that a further deactivation step is open in the triad to $PH_2^+ - Ir^- - PAu$. With respect to the dyad, where deactivation of the corresponding charge separated state $PH_2^+ - Ir^-$ can occur only by recombination to the ground state, deactivation in the triad can occur also via a further electron transfer step leading to the fully CS state $PH_2^+ - Ir - PAu^-$, with a rate of 1.2×10^{10} s^{-1} [44, 45]. The fully CS state is, therefore, formed with an efficiency of 0.5. Due to the high driving force of the recombination reaction ($\Delta G^0 = -1.55$ eV), we were expecting a slow recombination reaction, in accord with the so-called Marcus inverted behavior [46], characterised by a slowing down of the reaction by increasing driving force. The lifetime was, on the contrary, rather short, 3.5 ns and was determined by a rapid recombination to the triplet excited state localized on the porphyrin, $^3PH_2 - Ir - PAu$. Fast spin flip from a singlet CS state to a triplet CS state, which is the rate determining step for recombina-

tion to a triplet, is again a peculiarity of the arrays containing heavy atoms as Ir(III) [45].

With this in mind, we tried to avoid the presence of triplet excited states at lower energy than the target CS state. To this aim, we selected zinc porphyrin as an electron donor and photosensitizer in the triad $\mathbf{25}^{4+}$ (Fig. 8) [45, 47]. Zinc porphyrin has a triplet excited state approximately 0.1 eV higher in energy than the free base and has a lower oxidation potential, by ca. 0.2 V (which places the CS states involving oxidized zinc porphyrin at energies lower by the same 0.2 eV amount). The experiments for triad $\mathbf{25}^{4+}$ were carried out both in moderately polar (CH_2Cl_2) and in non-polar (toluene) solvents. The best results were obtained in toluene and the energy level diagram in this solvent is reported in Scheme 8. It can be immediately seen that in this case, compared to triad $\mathbf{24}^{4+}$, the situation is more favorable in that the triplet excited state ^{3}PZn – Ir – PAu is higher than the level of the CS state PZn^+ – Ir – PAu^-. Upon excitation of the zinc porphyrin unit, after a very fast quenching of the ^{1}PZn – Ir – PAu luminescence ($\tau < 20$ ps), PZn^+ – Ir – PAu^- formation is detected within the time resolution of the apparatus and decays with a lifetime of 450 ns. The results in dichloromethane were less satisfactory in that the fully CS state was not formed, due to the lack of driving force for the reaction leading from PZn^+ – Ir^- – PAu to PZn^+ – Ir – PAu^-. The difference in behavior of the triad in CH_2Cl_2 and toluene is due to the different polarity of the solvents which stabilizes the states in a remarkably different way [45].

The parameters of charge separation for the examined porphyrin based triads are collected in Table 2.

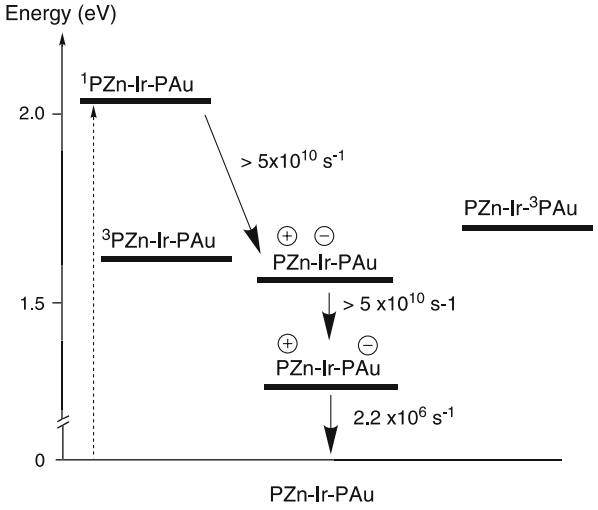

Scheme 8 Energy level diagram and reaction rates for the photoinduced processes occurring in triad $\mathbf{25}^{4+}$. The *dashed arrow* indicates excitation of the Zn porphyrin unit

Table 2 Properties of CS states formed in $Ru(terpy)_2^{2+}$ and $Ir(terpy)_2^{3+}$ complex-based triads containing porphyrins

Triad	Energy CS/eV	ϕ_{CS} [a]	τ_{CS}/ns
$\mathbf{6}^{3+}$	1.4	0.27	75
$\mathbf{7}^{3+}$	1.23	0.60	33
$\mathbf{24}^{4+}$	1.55	0.5	3.5
$\mathbf{25}^{4+}$	1.34	1	450

[a] Efficiency of CS; for the solvent employed and the experimental conditions see [22, 45]

2.4 Ir as Photoactive Centre

In the systems described above, a porphyrin is used as a photoactive centre, and the iridium complex acts only as a gathering metal and an electron relay. However the Ir(III) complex can also act as a photosensitizer if excited at a convenient wavelength. Indeed $Ir(terpy)_2^{3+}$ and derivatives (i) absorb moderately in the ultraviolet and high-energy visible region of the spectra, Table 1, (ii) the lowest excited state can store more energy than other photosensitizers, and (iii) have a remarkably long lifetime (see Sect. 2.2). For this reason we developed projects based on the use of iridium complex centres as photosensitizers.

The first experiments in this direction were carried out on the triads $\mathbf{24}^{4+}$ and $\mathbf{25}^{4+}$ (Fig. 8), by exciting preferentially the metal centre around 340–355 nm. Excitation at this wavelength region produces to a predominant extent the excited state localized on the iridium complex unit, the ligand centered triplets $PH_2 - {}^3Ir - PAu$ or $PZn - {}^3Ir - PAu$ [48]. Energy transfer to the porphyrin triplets dominates the deactivation of $PH_2 - {}^3Ir - PAu$ in $\mathbf{24}^{4+}$, with rate constants of 2.9×10^{10} s^{-1} for the transfer to the gold porphyrin localized excited state and ca. 10^{11} s^{-1} to the free base porphyrin localized excited state, respectively (Scheme 9).

This is in contrast to the results obtained following selective excitation of the PH_2 unit discussed above, and yielding a multi-step electron transfer leading to charge separation. The different outcome can be discussed on the basis of the overlap of the HOMO and LUMO orbitals involved in the electron transfer reaction for the Ir acceptor unit and the PH_2 donor unit, with the aid of semi-empirical calculations [48]. Remarkably, the zinc porphyrin based array $PZn - Ir - PAu$, $\mathbf{25}^{4+}$, displays an efficient electron transfer with the formation of a CS state with unitary yield also upon excitation of the iridium complex. This happens because the selective excitation of the zinc porphyrin chromophore discussed above, and the deactivation of the excited state $PZn - {}^3Ir - PAu$, follow the same paths as those reported in Scheme 8.

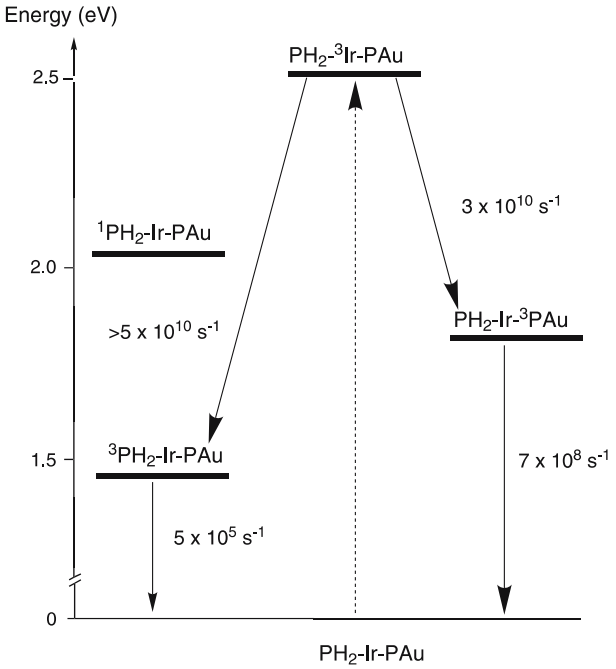

Scheme 9 Energy level diagram and reaction rates for the photoinduced processes occurring in compound $\mathbf{24}^{4+}$ following excitation of the Ir complex unit (*dashed arrow*)

A higher driving force for electron transfer in the case of $\mathbf{25}^{4+}$ compared to $\mathbf{24}^{4+}$ could explain the predominance of the electron transfer reaction with respect to energy transfer paths in the latter case.

A subsequent study dealt with system $\mathbf{26}^{4+}$, a pseudo-rotaxane incorporating an Ir(III) terpy-type complex and a copper(I) centre with a pseudo tetrahedral coordination provided by a macrocycle and a monosubstituted phenanthroline (Fig. 9) [36]. Following selective excitation of the iridium complex at 390 nm in this dyad, the emission is almost completely quenched. In principle, this could be due both to electron and/or to energy transfer. As discussed previously, Ir(III) bis-terpy type complexes are, in fact, rather strong oxidants in their ground states, $E_{1/2}$ ca. – 0.75 V vs SCE [49], whereas Cu(I)-phen-type complexes can easily oxidize to Cu(II), at a potential of ca. + 0.6 V vs SCE. The energy of the excited state stored on the Ir(III) complex could easily promote electron transfer from the iridium to the copper units, with a ΔG^0 of reaction of ca. – 1 eV. However energy transfer from the iridium to the copper unit (whose excited state lies at ca. 1.7 eV) is also thermodynamically feasible, with a ΔG^0 of ca. 0.8 eV. For the case of $\mathbf{26}^{3+}$, it was difficult to evaluate the relative weight of the two contributions, given that both 2,9-unsubstituted and unsymmetrically substituted bis-phenanthroline derivatives are non-emissive [50]. A further step is the modification of the

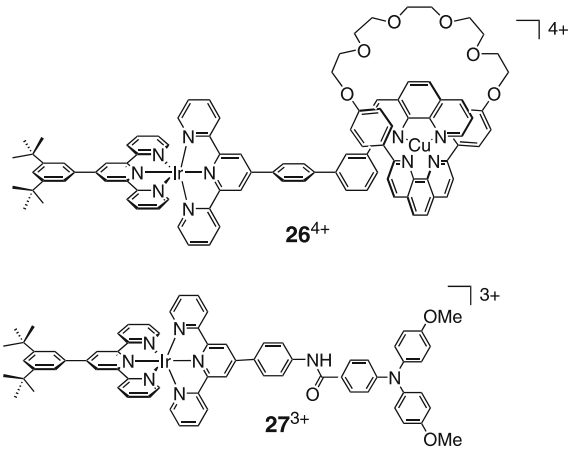

Fig. 9 Chemical structures of compounds $\mathbf{26}^{4+}$ and $\mathbf{27}^{3+}$

copper ligand in order to prepare a luminescent Cu(I)-bis-phenanthroline derivative. This would allow, without changing the thermodynamic parameters of the system, an investigation of the sensitization of the luminescence of the copper unit, shedding light on the nature of the process.

In order to eliminate possible energy transfer processes depleting the Ir complex excited state, dyad $\mathbf{27}^{3+}$ (Fig. 9), made of a triarylamine electron donor D linked to the iridium bis-terpyridine complex by an amido-phenyl group was synthesized and examined [51]. D can be oxidized at 0.8 V vs. SCE, and has an excited state energy at ca. 3 eV, higher than the energy of the photosensitizer excited state, preventing an energy transfer process from the iridium complex unit (Scheme 10).

Selective excitation of metal complex unit in $\mathbf{27}^{3+}$ resulted in a complete quenching of its luminescence with the formation within 20 ps of the CS state $Ir^- - D^+$. The latter, identified from the absorption band peaking at 765 nm, decays with a life-time of 70 ps. Excitation of the D component around 330 nm also resulted in a complete quenching of the triphenylamine luminescence to yield the same CS state. The quenching mechanism can be described as a reductive quenching when the Ir complex is excited, i.e., an electron moves from the HOMO localized on the donor to the HOMO localized on the Ir complex. By contrast, when the donor is excited, an electron moves from the LUMO localized on the donor to the LUMO of the Ir complex acceptor, very likely localized on the bridging terpyridine. The localization of the extra electron on the bridging ligand, very close to the oxidized donor group, could be the reason for the relatively short lifetime of this CS state. On the other hand, the proximity allows for the formation of the CS state with a unity yield. We are presently working on the addition to the iridium complex centre of an ancillary electron acceptor group able to undergo a further

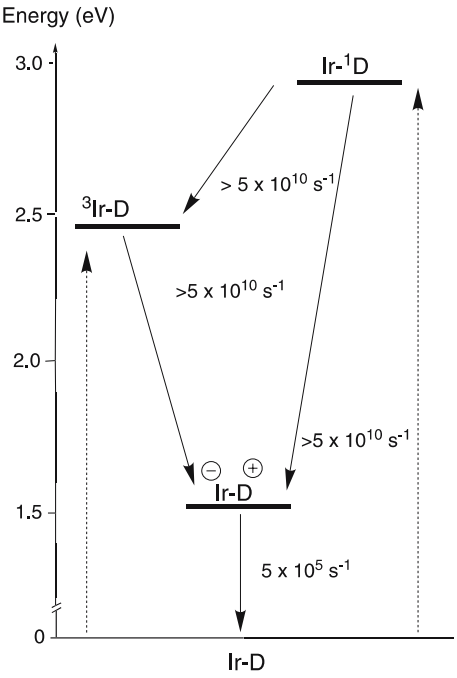

Scheme 10 Energy level diagram and reaction rates for the photoinduced processes occurring in the dyad $\mathbf{27}^{3+}$. The *dashed arrows* indicate excitation of both components

electron transfer step. This should increase the separation between the hole and the electron in the final charge separated state and hopefully slow down the recombination event.

2.5 Related Systems Reported by Other Groups

In view of the development of chemical approaches to artificial photosynthesis, there are several possible ways towards multicomponent systems incorporating metal complex units [52, 53]. For instance, new types of metal centres can prove amenable to the preparation of assemblies suited for the study of CS and CR events. This is the case of the triadic systems built around an acetylide-Pt(II)-terpy centre, $\mathbf{28}^{+}$ and related systems (Fig. 10) [54]. For $\mathbf{28}^{+}$, the energy content of the excited metal complex core is ca. 2.2 eV, and this energy can drive formation of a fully CS state, ending up with oxidation of the PTZ unit and reduction of the tterpy-nitrostilbene ligand. The CS state lives 230 ns and is formed with an efficiency of 25–30%.

Finally, it is of worth recalling the continuing development of systems based on Ru(II)-tris-bidentate chromophores. Above, we have pointed out that this chromophore has limitations regarding both the stored energy con-

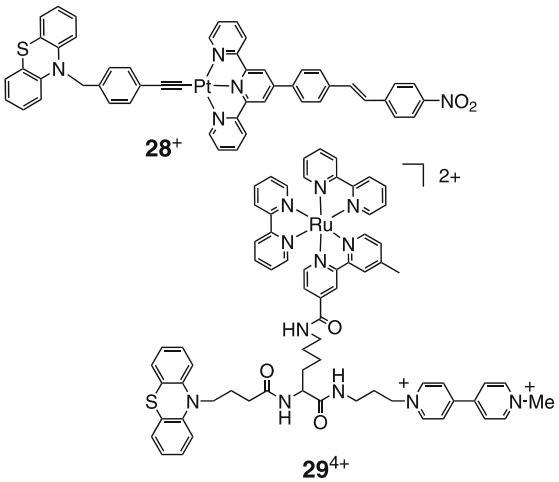

Fig. 10 Chemical structures of compounds $\mathbf{28}^{+}$ and $\mathbf{29}^{2+}$

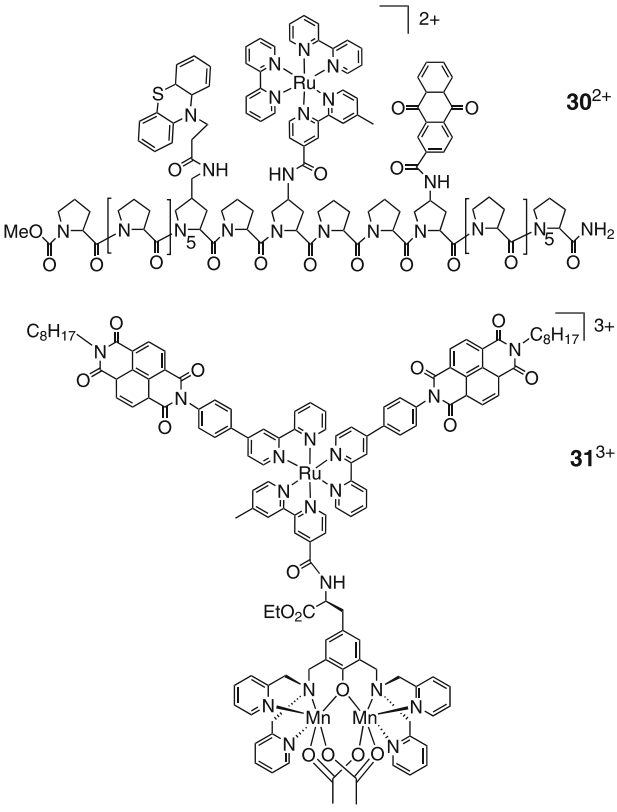

Fig. 11 Chemical structures of compounds $\mathbf{30}^{2+}$ and $\mathbf{31}^{3+}$

tent and the unfavourable geometric properties that do not allow a convenient spatial control of the products of the photoinduced events. However it is worth mentioning the work of Meyer and coworkers concerning the preparation of the lysine-based triadic system $\mathbf{29}^{4+}$, Fig. 10 [55] and of large molecular assemblies similar to $\mathbf{30}^{2+}$ in Fig. 11 [28, 53]. For the donor-chromophore-acceptor system $\mathbf{29}^{4+}$, excitation at metal-chromophore yields a PTZ^{+}-MV^{+} CS state with an efficiency of 0.34, which lives ca. 150 ns. Likewise, for the proline assembly $\mathbf{30}^{2+}$, MLCT excitation leads to simultaneous appearance of transient absorption features due to the PTZ radical cation and the anthraquinone radical anion. This fully CS state is formed with a 53% efficiency, stores 1.65 eV, and lives 175 ns (Fig. 11).

In addition, very recently it has been reported a $\tau = 600\ \mu s$ at room temperature (and 0.1–1 s at 140 K), for a CS state formed upon light absorption in the multicomponent system $Mn_2(II, II)$ – Ru – NDI $\mathbf{31}^{3+}$, including a manganese dimer moiety ($Mn_2(II, II)$), and two naphthalenediimide (NDI) units, Fig. 11 [56]. The photoinduced events are driven by light absorption at the $Ru(bpy)_3^{2+}$ photosensitizing unit, resulting in oxidation of the manganese dimer, $Mn_2(II, III)$ and NDI reduction. This outstanding result was explained in terms of the Marcus theory [46], based on the unusually large reorganization energy (2 eV) for the CR step, due in turn to the large inner reorganization energy of the manganese dimer.

3
Ruthenium-based Light-driven Molecular Machine Prototypes

3.1
Use of Dissociative Excited States to Set Ru(II)-complexed Molecular Machines in Motion: Principle

Light irradiation has recently been reported to produce molecular motions, either alone or in conjunction with a redox chemical reaction [57–69]. Pure photonic stimuli are particularly promising as the system in motion is not altered by the addition of chemicals; however, only a few examples have been reported. Among the light-driven molecular machine prototypes which have been described in the course of the last few years, a very distinct family of dynamic molecular systems takes advantage of the dissociative character of ligand-field states in $Ru(diimine)_3^{2+}$ complexes [70–76]. In these compounds, one part of the system is set in motion by photochemically expelling a given chelate, the reverse motion being performed simply by heating the product of the photochemical reaction so as to regenerate the original state. In these systems, the light-driven motions are based on the formation of dissociative excited states. Complexes of the $Ru(diimine)_3^{2+}$ family are particularly well adapted to this approach. If distortion of the coordination octahedron is suffi-

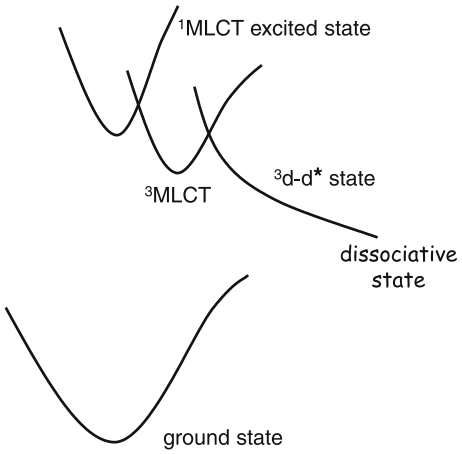

Fig. 12 The ligand-field state ^3d–d^* can be populated from the ^{3}MLCT state, provided the energy difference between these two states is not too large: formation of this dissociative state leads to dissociation of a ligand

cient to significantly decrease the ligand field, which can be realized by using one or several sterically hindering ligands, the strongly dissociative ligand-field state (^3d–d state) can be efficiently populated from the metal-to-ligand charge transfer (^{3}MLCT) state to result in expulsion of a given ligand. The principle of the whole process is represented in Fig. 12.

It is, thus, important that the ruthenium(II) complexes that are to be used as building blocks of the future machines contain sterically hindering chelates so as to force the coordination sphere of the metal to be distorted from the perfect octahedral geometry. We will discuss the photochemical reactivity of rotaxanes and catenanes of this family as well as non-interlocking systems like scorpionates since the lability of bulky monodentate ligands could also lead to useful photosubstitution reactions.

3.2 Photochemical and Thermal Ligand Exchange in a Ruthenium(II) Complex Based on a Scorpionate Terpyridine Ligand

Among the numerous ruthenium(II) complexes described in the literature, several lead to interesting photolabilisation reactions that are both efficient and selective [71–80]. For example, Ru(tterpy)(dmbp)(L)$^{2+}$, (L = pyridine or CH_3CN) undergoes a reversible interchange of the sixth ligand L under visible light irradiation [81] (Scheme 11).

In order to investigate such systems further, we have prepared and characterised a series of ruthenium(II) complexes of the type Ru(terpy)(phen)(L)$^{2+}$ in which L is a monodentate ligand such as pyridine, 2-isoquinoline,

(1) $Ru(tterpy)(dmbp)(CH_3CN)^{2+} \xrightarrow{h\nu,\ py} Ru(tterpy)(dmbp)(py)^{2+} + CH_3CN$

(2) $Ru(tterpy)(dmbp)(py)^{2+} \xrightarrow{h\nu,\ CH_3CN} Ru(tterpy)(dmbp)(CH_3CN)^{2+} + py$

Scheme 11 Equations of the interchange of the sixth ligand L in the $Ru(tterpy)(dmbp)(L)^{2+}$ type complexes

4-dimethylaminopyridine, 4-(4′-methyl-pyridinium)-pyridine, phenothiazine, DMSO, CH_3CN, 4-methoxy-benzonitrile and H_2O [82]. Our investigations of these complexes show that the nitrile ligand in $Ru(terpy)(phen)(CH_3CN)^{2+}$ can be selectively photo-expelled and replaced by H_2O under visible light irradiation in an acetone-water mixture (85 : 15, v/v). This process has been monitored by UV-visible and ^1H NMR spectroscopy. Both techniques demonstrate that the photochemical reaction is highly selective and quantitative. The reverse reaction, i.e., the thermal recoordination of an acetonitrile molecule, also takes place quantitatively at room temperature. We have also observed that a similar photochemical reaction occurs for the substitution of CH_3CN by pyridine. We have proposed, therefore, a system that combines the general properties of scorpionate ligands with the ability of ruthenium(II) complexes to undergo ligand exchange under light irradiation [83]. The ruthenium complex $\mathbf{32}^{2+}$ in which a benzonitrile group is tethered to the terpyridine subunit (Fig. 13) has been prepared.

In this complex, the benzonitrile coordinating group can be photoexpelled and thermally recoordinated. The effect of tethering the benzonitrile group is to facilitate the recoordination of the nitrile functionality, since the effective concentration of the nitrile in the scorpionate complex is expected to be higher than if it were free in the bulk of the solution. The photolabilisation of the benzonitrile arm has initially been examined in pyridine solution. Both ^1H NMR and UV-visible measurements show that the reaction is clean and quantitative. Due to the strong coordination ability of pyridine it was not possible to restore the starting compound either thermally or photochemically. By contrast, a reversible system was obtained in acetone-H_2O mixture. At a low concentration of $\mathbf{32}^{2+}$ in acetone : water (85 : 15 v/v) the monitoring of the photochemical reaction by electronic absorption spectroscopy and TLC clearly indicates the complete disappearance of $\mathbf{32}^{2+}$ (λ_{max} = 454 nm) and the simultaneous appearance of the aqua-form (λ_{max} = 490 nm). By ^1H NMR, in a more concentrated solution (10^{-3} M), a stationary equilibrium is reached. The nature of the reaction product has also been unambiguously confirmed by ES-MS spectroscopy (peak at 939.2 for the aqua form; calculated for M-PF_6 = 939.0). The thermal recoordination of the nitrile arm takes places slowly at room temperature (82% of recovery in one day) or faster by heating the mixture at reflux for 1 h. At this concentration no by-product resulting from intermolecular complexation has been detected.

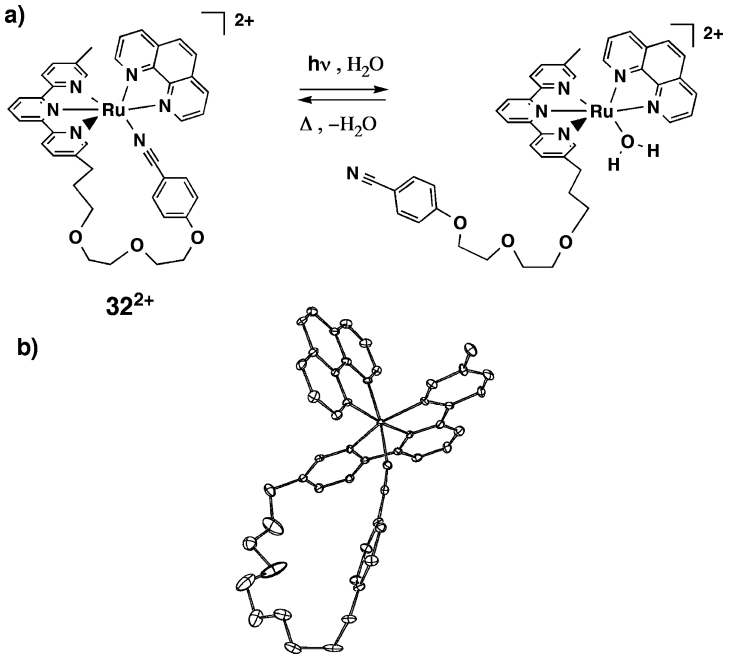

Fig. 13 **a** Photolabilisation and thermal recoordination of complex $\mathbf{32}^{2+}$. **b** ORTEP view of the ruthenium complex $\mathbf{32}^{2+}$. Ellipsoids are scaled to enclose 30% of the electronic density

3.3
A Ru(terpy)(phen)-incorporating Ring and Its Light-induced Geometrical Changes

A particularly promising feature of the Ru(terpy)(phen)$(L)^{2+}$ series, in relation to future molecular machine and motors, is related to the pronounced effect of steric factors on the photochemical reactivity of the complexes [84]. When the bulkiness of the spectator phenanthroline moiety was increased, the steric congestion of the coordination sphere of the ruthenium complex also increased. This increased congestion was qualitatively correlated to the enhanced photoreactivities of these complexes (Fig. 14). More specifically, changing phen for dmp increased by one to two orders of magnitude the quantum yield of the photosubstitution reaction of L by pyridine with L = dimethylsulfide or 2,6-dimethoxybenzonitrile.

In the most congested case, $(Ru(terpy^*)(dmp)(CH_3SCH_3)^{2+})$, the photosubstitution quantum yield was shown to be $\phi = 0.36$ at room temperature in pyridine, which is an extremely high value in ruthenium(II) photochemistry. The control of the bulkiness of the spectator chelates, leading to the control of the congestion of the complex and, hence, to the efficiency of ligand photoexpulsion, is a specific feature of the Ru(terpy)(phen)$(L)^{2+}$ core. This

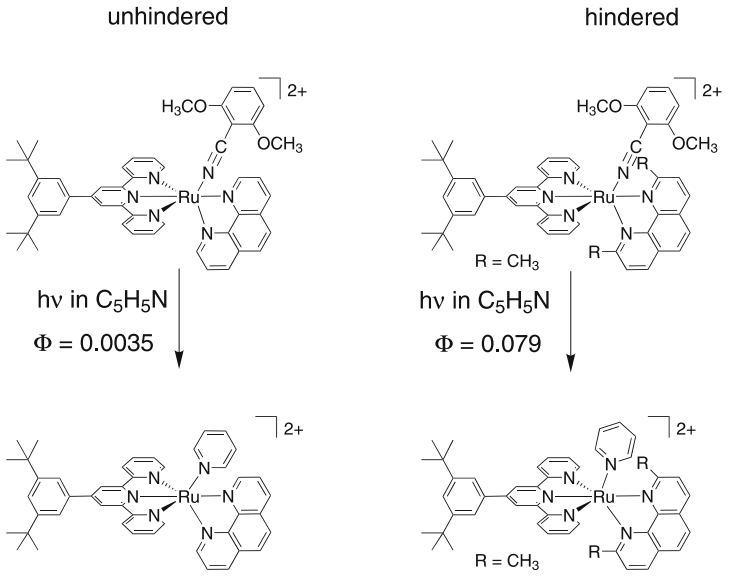

Fig. 14 Photosubstitution quantum yield with the hindered dmp spectator chelate compared to its unhindered analog phen. Quantum yield values are given at room temperature in neat pyridine

new property, added to the potential variety of monodentate ligands L and to the expected mildness of thermal back-coordination conditions, makes the Ru(terpy)(phen)(L)$^{2+}$ family a highly promising photoactive core for elaborating future light-driven molecular machine.

Rings are essential components of molecular machine prototypes, especially within the catenane family [85]. A limited number of ruthenium(II)-incorporating macrorings have been made [86–89]. Since Ru(II) is substitutionally inert, the so-called self-assembly approach cannot be utilized [90]. Recently, we synthesized a novel Ru(II)-containing cycle, the ligand set consisting of a terpy derivative and a phen chelate. The sixth ligand can thermally or photochemically be substituted by another monodentate ligand [81, 91]. It consists of pyridine (py), acetonitrile or S-linked DMSO. In addition, a new photoisomerisation reaction of the ruthenium(II) complex leads to a dramatic change of the ring shape under the action of visible light, the reverse process regenerating the initial state by a thermal reaction. An example of the substitution-isomerisation in an acyclic complex is shown in Fig. 15.

The embedding of a Ru(terpy)(phen)$^{2+}$ moiety in a ring is certainly not trivial since the terpy fragment occupies three meridional sites of the metal octahedron and the phen chelate is almost opposite to the terpy in the metal coordination sphere. We thought that a convenient way to connect the phen and the terpy fragments was to interlink a lateral position of the phen (3 position) and the para position (4′) of the central pyridinic nitrogen atom of

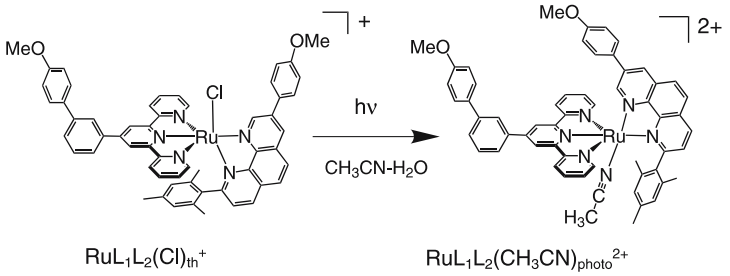

Fig. 15 Photosubstitution-isomerisation processes in $Ru(L_1)(L_2)(Cl)^+$ complex

the terpy. This strategy should allow the formation of a large ruthenium(II)-containing ring.

A sequence of reactions, including the ring closing metathesis (RCM) reaction, leads to a 39-membered ring $\mathbf{33}^{2+}_{photo}$ in the overall yield of 70% as depicted in Fig. 16. Although the photoisomers are very inert towards isomerisation for all the members of the family, a procedure was discovered which allowed for conversion of the photoisomer $\mathbf{33}^{2+}_{photo}$ to the thermal isomer $\mathbf{33}^{2+}_{th}$. This procedure is quite general and can also be applied to acyclic complexes. The reaction is represented in a very schematic fashion in Fig. 16. It has been carried out with either pyridine or CH_3CN as the entering ligand from the intermediate DMSO complex.

The conversion of $\mathbf{33}^{2+}_{photo}$ to $\mathbf{33}^{2+}_{th}$ is performed in two steps: 1) substitution of py by DMSO and isomerisation, 2) substitution of DMSO by py. Its overall yield is above 80%. In order to perform a complete cycle, the photochemical reaction leading back to $\mathbf{33}^{2+}_{photo}$ was carried out in the usual way (irradiation performed at room temperature with a 1000 W xenon arc-lamp filtered by a water filter) in pyridine. It turned out to be virtually quantitative.

This photochemical/thermal isomerisation of the ruthenium-containing ring is accompanied by a dramatic geometrical change of the compound. Molecular modelling studies [92] suggest that the distance between the two

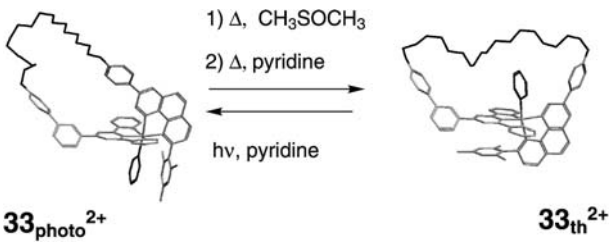

Fig. 16 Thermal isomerisation of the photoisomer $\mathbf{33}^{2+}_{photo}$ and the photochemical back reaction. The pyridine ligand moves from an external position to an intra-ring location while the $-(CH_2)_{18}-$ fragment undergoes a folding/unfolding process

oxygen atoms borne by the phenyl rings of the terpy and phen ligands varies from 9.7 Å for the photochemical isomer $\mathbf{33}^{2+}_{photo}$ to 17.7 Å for $\mathbf{33}^{2+}_{th}$. The $-(CH_2)-_{18}$ linker, which connects these two oxygen atoms, undergoes a folding/stretching process, as depicted in Fig. 16. In the past, the photochemical cis-trans isomerisation of an azo ($-N=N-$) bond has been used to modify the shape of cyclic compounds [93]. Related geometrical changes have also been triggered by chemical means, in dinuclear copper(II) complexes [94].

3.4 Light-driven Unthreading Reaction in Rotaxane with a $[Ru(diimine)_3]^{2+}$ Core

We have recently reported the synthesis of a [2]rotaxane constructed around a $Ru(diimine)^{2+}_3$ core [95]. The ring was a derivative of dmbp, and, in the course of the threading reaction, we noticed that both exo- and endo-coordination to the ruthenium(II) centre of the rod-like fragment take place, as schematically represented in Fig. 17.

In order to circumvent this synthetic difficulty, we replaced the dmbp motif by a 6,6′-diphenyl-2,2′-bipyridine chelate (dpbp), which provides the system with much better geometrical control. According to CPK models, exo coordination of a dpbp-incorporating ring is virtually impossible, except with very large rings. This approach turned out successful since the desired rotaxane and its non-stoppered analogue could be prepared in good yield, without formation of exo-coordinated species (Fig. 18). In addition, the photochemical behaviours of these compounds have shown that the ring is efficiently decoordinated from the ruthenium(II) centre under visible light irradiation. In a first step, we studied the photochemical behaviour of complex $\mathbf{34}^{2+}$. By irradiating a solution of $\mathbf{34}^{2+}.2PF_6^-$ in 1,2-dichloroethane, using a band pass filter centered at around 470 nm and in the presence of a large excess of Cl^-, a clean photochemical reaction takes place. The photoinduced "unthreading" reaction was monitored by UV-vis spectroscopy. The series of visible spectra, characteristic of metal-to-ligand charge transfer (MLCT) bands, is given in Fig. 19.

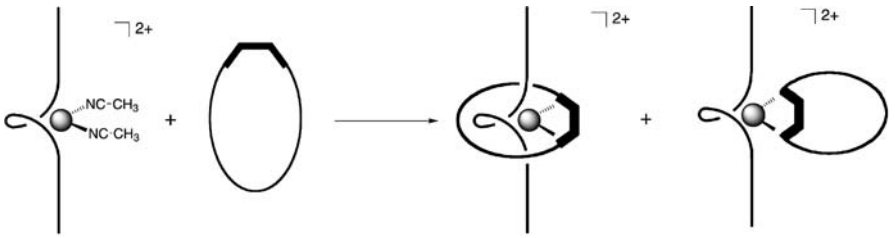

Fig. 17 Synthesis of a pseudo-rotaxane and its *exo*-isomer

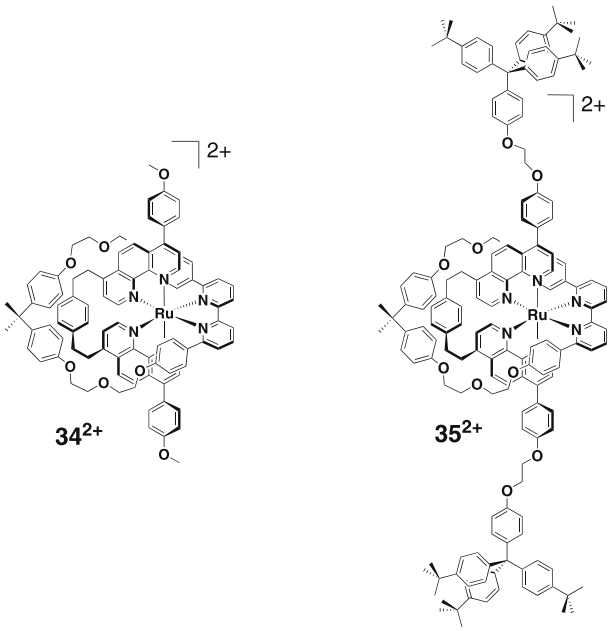

Fig. 18 Formulae of the pseudo-rotaxane 34^{2+} and of the rotaxane 35^{2+}

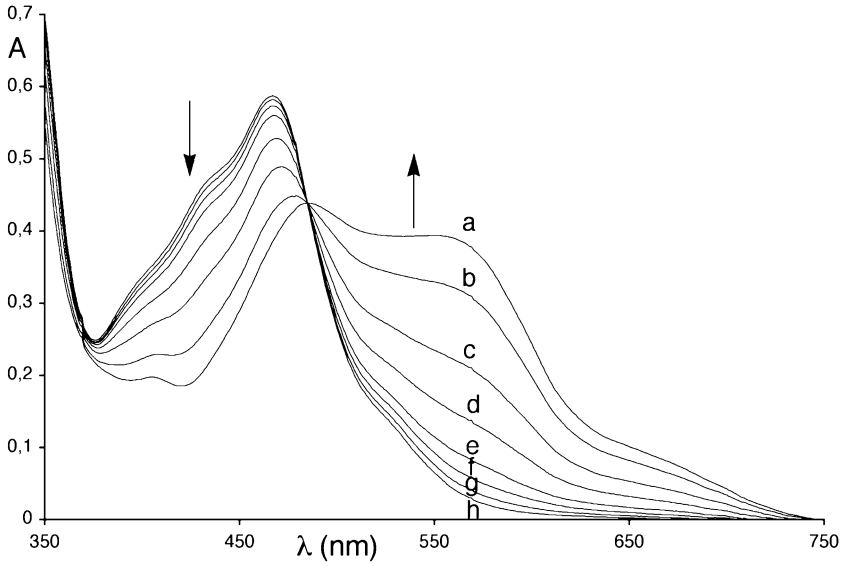

Fig. 19 Absorption spectra (visible region) of a solution containing 34^{2+} and $NEt_4{}^+Cl^-$ in $ClCH_2CH_2Cl$ before, during, and after irradiation. Spectra were recorded at $t = 0$ s **a**, 15 s **b**, 40 s **c**, 90 s **d**, 200 s **e**, 400 s **f**, 900 s **g**, 2400 s **h**

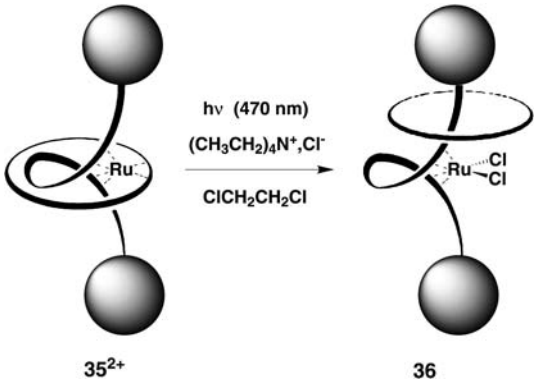

Fig. 20 Schematic representation of the photochemical reaction leading to the disconnected rotaxane **36**

From a band centered at 465 nm, typical of a Ru(diimine)$_3^{2+}$ complex [96], a new spectrum is obtained by irradiation, which corresponds to a $RuCl_2$ (diimine)$_2$ complex (λ_{max} = 562 nm). As expected, the MLCT band for the photochemical product is strongly bathochromically shifted from that of the tris-diimine complex. The presence of a clean isosbestic point at 485 nm indicates that the photochemical reaction is selective and quantitative. This has been confirmed by ^{1}H NMR spectroscopy and by thin-layer chromatography. Only one photochemical product was detected and the starting complex **34**$^{2+}$ has completely disappeared. Similar experiments have been performed with the rotaxane **35**$^{2+}$. The reaction is represented in a schematic fashion in Fig. 20.

The photochemical decoordination of the ring in **35**$^{2+}$ is also selective and clean. Here again, in an analogous way as with **34**$^{2+}$, an isosbestic point is observed at 486 nm. Thin-layer chromatography turned out to be particularly useful to monitor the reaction. It showed that **35**$^{2+}$.2PF_6^- is gradually converted to a single purple complex, **36**, under irradiation (470 nm). Importantly, traces of the free ring could not be detected, demonstrating that both forms of the rotaxane, **35**$^{2+}$ and **36**, do not undergo unthreading, even to a minor extent. Unfortunately, the thermal recoordination reaction of the ring to lead back to **35**$^{2+}$ is not as clean and selective as the presently described threading reaction used to prepared **34**$^{2+}$ nor as in the case of a related catenane (see next paragraph).

3.5 Photoinduced Decoordination and Thermal Recoordination of a Ring in a Ruthenium(II)-Containing [2]Catenane

For this latter system, the synthetic approach is based on the template effect of an octahedral ruthenium(II) centre [97–100]. Two 1,10-phenanthroline ligands are incorporated in a ring, affording the precursor to the catenane. The

main point of the design is the observation that it should be possible to incorporate two bidentate chelates of the octahedron in a ring and subsequently to thread a fragment containing the third chelate through the ring. This second process would of course be driven by coordination to the central metal. The synthetic procedure starts with the preparation of a large ring incorporating two phen units [99, 100]. The choice of the ring was dictated by CPK models and by synthesis considerations. The [2]catenanes $\mathbf{37}^{2+}$ and $\mathbf{38}^{2+}$, which differ essentially by the size of the ring incorporating the ruthenium core, are represented in Fig. 21. Compound $\mathbf{37}^{2+}$ consists of a 50-membered ring which incorporates two phen units and a 42-membered ring which contains the bpy chelate. Compound $\mathbf{38}^{2+}$ contains the same bpy-incorporating ring as $\mathbf{37}^{2+}$, but the other ring is a 63-membered ring. Clearly, from CPK model considerations, $\mathbf{38}^{2+}$ is more adapted than $\mathbf{37}^{2+}$ to molecular motions in which both constitutive rings would move with respect to one another since the situation is relatively tight for the latter catenane. The light-induced motion and the thermal back reaction carried out with $\mathbf{37}^{2+}$ or $\mathbf{38}^{2+}$ are represented in Fig. 21. They are both quantitative, as shown by UV/Vis measurements and by ^{1}H NMR spectroscopy.

The photoproducts, [2]catenanes $\mathbf{37}'$ and $\mathbf{38}'$, contain two disconnected rings since the photochemical reaction leads to decomplexation of the bpy chelate from the ruthenium(II) centre. In a typical reaction, a degassed CH_2Cl_2 solution of $\mathbf{38}^{2+}$ and $NEt_4^+.Cl^-$ was irradiated with visible light, at

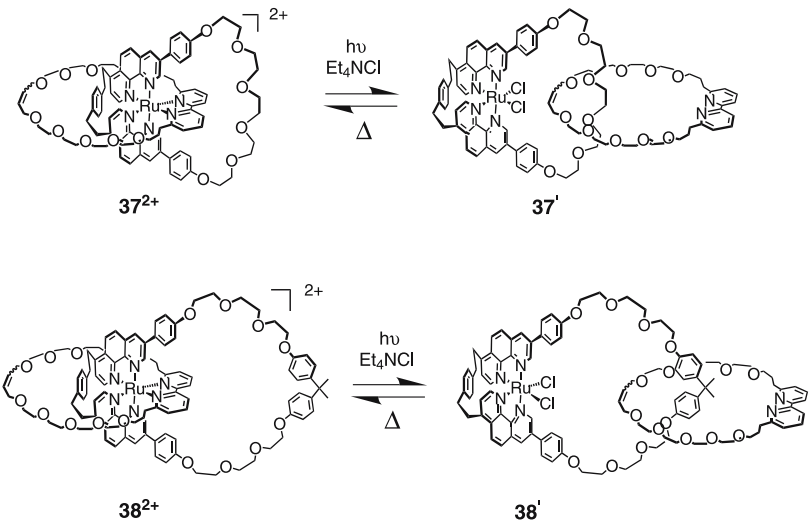

Fig. 21 Catenanes $\mathbf{37}^{2+}$ or $\mathbf{38}^{2+}$ undergo a complete rearrangement by visible light irradiation: the bpy-containing ring is efficiently decoordinated in the presence of Cl^-. By heating the photo-products $\mathbf{37}'$ or $\mathbf{38}'$, the starting complexes $\mathbf{37}^{2+}$ or $\mathbf{38}^{2+}$ are quantitatively regenerated

room temperature. The colour of the solution rapidly changed from red ($\mathbf{38}^{2+}$: λ_{max} = 458 nm) to purple ($\mathbf{38}'$: λ_{max} = 561 nm) and after a few minutes the reaction was complete. The recoordination reaction $\mathbf{38}' \rightarrow \mathbf{38}^{2+}$ was carried out by heating a solution of $\mathbf{38}'$. The quantum yield for the photochemical reaction $\mathbf{38}^{2+} \rightarrow \mathbf{38}'$ at 25 °C and λ = 470 nm (±50 nm) can be very roughly estimated as 0.014 ± 0.005. One of the weak points of the present system is certainly the limited control over the shape of the photoproduct since the decoordinated ring can occupy several positions. It is hoped that, in the future, an additional tuneable interaction between the two rings of the present catenanes, $\mathbf{37}'$ or $\mathbf{38}'$ will allow better control over the geometry of the whole system. In parallel, two-colour machines will be elaborated, for which both motions will be driven by photonic signals operating at different wavelengths.

4 Conclusion

The modern tools available in synthetic chemistry, either from the organic viewpoint or concerning the preparation of transition metal complexes, allow one to prepare more and more sophisticated molecular systems. In parallel, time-resolved photochemistry and photophysics are nowadays particularly efficient to disentangle complex photochemical processes taking place on multicomponent molecules. In the present chapter, we have shown that the combination of the two types of expertise, namely synthesis and photochemistry, permits to tackle ambitious problems related to artificial photosynthesis or controlled dynamic systems. Although the two families of compounds made and studied lead to completely different properties and, potentially, to applications in very remote directions, the structural analogy of the complexes used is striking.

In the course of the last three decades, the archetype $Ru(bpy)_3^{2+}$ has been at the origin of an extremely active field of research aimed at converting light energy into chemical energy. It has also been used more recently by a few groups to fabricate light-driven molecular machines.

1. $Ir(terpy)_2^{3+}$ is reminiscent of $Ru(bpy)_3^{2+}$ by some of its photochemical properties but, it is at the same time very different as far as its geometrical properties are concerned and for its electronic and photochemical characteristics. This complex has been used both as a chromophore and as an electron relay, in relation to charge separation. It is expected that, in the future, long-lived charge-separated states will be obtained by constructing carefully designed molecular triads with an $Ir(terpy)_2^{3+}$ central core.
2. $[RuL^1L^2L^3]^{2+}$ leads to photochemically labile complexes, able to undergo controlled ligand substitution under light irradiation, provided the three diimine chelates L^n have been selected in the proper way. Such systems,

once incorporated in rotaxanes or catenanes, represent promising light-driven molecular machine prototypes.

Acknowledgements We would like to thank all the very talented and enthusiastic researchers who participated in the work discussed in the present review article. Their names appear in the references. We thank CNR of Italy (PM-P04-ISTM-C1/ISOF-M5), CNRS (France), Ministero dell'Istruzione, dell'Universita' e della Ricerca of Italy (FIRB, RBNE019H9K) and COST D31 for financial support. SB acknowledges the Région Alsace for financial support.

References

1. Balzani V, Carassiti V (1970) Photochemistry of Coordination Compounds. Academic Press, London
2. Balzani V, Moggi L (1990) Coord Chem Rev 97:313
3. Gafney HD, Adamson AW (1972) J Am Chem Soc 94:8238
4. Juris A, Balzani V, Barigelletti F, Campagna S, Belser P, von Zelewsky A (1988) Coord Chem Rev 84:85
5. Danielson E, Elliott CM, Merkert JW, Meyer TJ (1987) J Am Chem Soc 109:2519
6. Di Marco G, Lanza M, Mamo A, Stefio I, Di Pietro C, Romeo G, Campagna S (1998) Anal Chem 70:5019
7. Gao RM, Ho DG, Hernandez B, Selke M, Murphy D, Djurovich PI, Thompson ME (2002) J Am Chem Soc 124:14828
8. Lo KKW, Chung CK, Lee TKM, Lui LH, Tsang KHK, Zhu NY (2003) Inorg Chem 42:6886
9. Adachi C, Baldo MA, Forrest SR, Thompson ME (2000) Appl Phys Lett 77:904
10. Lamansky S, Djurovich P, Murphy D, Abdel-Razzaq F, Lee HE, Adachi C, Burrows PE, Forrest SR, Thompson ME (2001) J Am Chem Soc 123:4304
11. Tsuboyama A, Iwawaki H, Furugori M, Mukaide T, Kamatani J, Igawa S, Moriyama T, Miura S, Takiguchi T, Okada S, Hoshino M, Ueno K (2003) J Am Chem Soc 125:12971
12. Gong X, Ostrowski JC, Moses D, Bazan GC, Heeger AJ (2003) Adv Funct Mat 13:439
13. Nazeeruddin MK, Humphry-Baker R, Berner D, Rivier S, Zuppiroli L, Graetzel M (2003) J Am Chem Soc 125:8790
14. Beeby A, Bettington S, Samuel IDW, Wang ZJ (2003) J Mater Chem 13:80
15. Holder E, Langeveld BMW, Schubert US (2005) Adv Mater 17:1109
16. Holder E, Marin V, Kozodaev D, Meier MAR, Lohmeijer BGG, Schubert US (2005) Macromol Chem Phys 206:989
17. Leslie W, Poole RA, Murray PR, Yellowlees LJ, Beeby A, Williams JAG (2004) Polyhedron 23:2769
18. Sajoto T, Djurovich PI, Tamayo A, Yousufuddin M, Bau R, Thompson ME, Holmes RJ, Forrest SR (2005) Inorg Chem 44:7992
19. Yang CH, Li SW, Chi Y, Cheng YM, Yeh YS, Chou PT, Lee GH, Wang CH, Shu CF (2005) Inorg Chem 44:7770
20. Collin JP, Guillerez S, Sauvage JP, Barigelletti F, De Cola L, Flamigni L, Balzani V (1991) Inorg Chem 30:4230
21. Collin JP, Guillerez S, Sauvage JP, Barigelletti F, De Cola L, Flamigni L, Balzani V (1992) Inorg Chem 31:4112
22. Harriman A, Odobel F, Sauvage JP (1995) J Am Chem Soc 117:9461

23. Andreasson J, Kodis G, Lin S, Moore AL, Moore TA, Gust D, Martensson J, Albinsson B (2002) Photochem Photobiol 76:47
24. Flamigni L, Barigelletti F, Armaroli N, Collin JP, Sauvage JP, Williams JAG (1998) Chem Eur J 4:1744
25. Flamigni L, Armaroli N, Barigelletti F, Balzani V, Collin JP, Dalbavie JO, Heitz V, Sauvage JP (1997) J Phys Chem B 101:5936
26. Sauvage JP, Collin JP, Chambron JC, Guillerez S, Coudret C, Balzani V, Barigelletti F, De Cola L, Flamigni L (1994) Chem Rev 94:993
27. Flamigni L, Barigelletti F, Armaroli N, Ventura B, Collin JP, Sauvage JP, Williams JAG (1999) Inorg Chem 38:661
28. Huynh MHV, Dattelbaum DM, Meyer TJ (2005) Coord Chem Rev 249:457
29. Kober EM, Caspar JV, Lumpkin RS, Meyer TJ (1986) J Phys Chem 90:3722
30. Treadway JA, Chen PY, Rutherford TJ, Keene FR, Meyer TJ (1997) J Phys Chem A 101:6824
31. Goze C, Chambron JC, Heitz V, Pomeranc D, Salom-Roig XJ, Sauvage JP, Morales AF, Barigelletti F (2003) Eur J Inorg Chem, p 3752
32. Flynn CM Jr, Demas JN (1974) J Am Chem Soc 96:1959
33. Demas JN, Harris EW, Flynn CM, Diemente D (1975) J Am Chem Soc 97:3838
34. Collin JP, Dixon IM, Sauvage JP, Williams JAG, Barigelletti F, Flamigni L (1999) J Am Chem Soc 121:5009
35. Flamigni L, Ventura B, Barigelletti F, Baranoff E, Collin JP, Sauvage JP (2005) Eur J Inorg Chem, p 1312
36. Baranoff E, Griffiths K, Collin JP, Sauvage JP, Ventura B, Flamigni L (2004) New J Chem 28:1091
37. De Cola L, Balzani V, Barigelletti F, Flamigni L, Belser P, Vonzelewsky A, Frank M, Vogtle F (1993) Inorg Chem 32:5228
38. Guardigli M, Flamigni L, Barigelletti F, Richards CSW, Ward MD (1996) J Phys Chem 100:10620
39. Stone ML, Crosby GA (1981) Chem Phys Lett 79:169
40. Passalacqua R, Loiseau F, Campagna S, Fang YQ, Hanan GS (2003) Angew Chem Int Ed 42:1608
41. Wang JH, Hanan GS, Loiseau F, Campagna S (2004) Chem Commun, p 2068
42. Medlycott EA, Hanan GS (2005) Chem Soc Rev 34:133
43. Abrahamsson M, Wolpher H, Johansson O, Larsson J, Kritikos M, Eriksson L, Norrby PO, Bergquist J, Sun LC, Akermark B, Hammarström L (2005) Inorg Chem 44:3215
44. Dixon IM, Collin JP, Sauvage JP, Barigelletti F, Flamigni L (2000) Angew Chem Int Edit 39:1292
45. Dixon IM, Collin JP, Sauvage JP, Flamigni L (2001) Inorg Chem 40:5507
46. Marcus RA (1993) Angew Chem Int Ed 32:1111
47. Flamigni L, Dixon IM, Collin JP, Sauvage JP (2000) Chem Commun, p 2479
48. Flamigni L, Marconi G, Dixon IM, Collin JP, Sauvage JP (2002) J Phys Chem B 106:6663
49. Dixon IM, Collin JP, Sauvage JP, Flamigni L, Encinas S, Barigelletti F (2000) Chem Soc Rev 29:385
50. Dietrich-Buchecker CO, Nierengarten JF, Sauvage JP, Armaroli N, Balzani V, De Cola L (1993) J Am Chem Soc 115:11237
51. Baranoff E, Dixon IM, Collin JP, Sauvage JP, Ventura B, Flamigni L (2004) Inorg Chem 43:3057
52. Eisenberg R, Nocera DG (2005) Inorg Chem 44:6799

53. Alstrum-Acevedo JH, Brennaman MK, Meyer TJ (2005) Inorg Chem 44:6802
54. Chakraborty S, Wadas TJ, Hester H, Schmehl R, Eisenberg R (2005) Inorg Chem 44:6865
55. Mecklenburg SL, Peek BM, Erickson BW, Meyer TJ (1991) J Am Chem Soc 113:8540
56. Borgström M, Shaikh N, Johansson O, Anderlund MF, Styring S, Akermark B, Magnuson A, Hammarström L (2005) J Am Chem Soc 127:17504
57. Livoreil A, Sauvage J-P, Armaroli N, Balzani V, Flamigni L, Ventura B (1997) J Am Chem Soc 119:12114
58. Armaroli N, Balzani V, Collin J-P, Gaviña P, Sauvage J-P, Ventura B (1999) J Am Chem Soc 121:4397
59. Mobian P, Kern J-M, Sauvage J-P (2004) Angew Chem Int Ed 43:2392
60. Koumura N, Geertsema EM, v Gelder MB, Meetsma A, Feringa BL (2002) J Am Chem Soc 124:5037
61. Koumura N, Zijistra RWJ, van Delden RA, Harada N, Feringa BL (1999) Nature 401:152
62. ter Wiel MKJ, van Delden RA, Meetsma A, Feringa BL (2003) J Am Chem Soc 125:15076
63. Norikane Y, Tamaoki N (2004) Organic Lett 6:2595
64. Muraoka T, Kinbara K, Kabayashi Y, Aida T (2003) J Am Chem Soc 125:5612
65. Kojima T, Sakamoto T, Matsuda Y (2004) Inorg Chem 43:2243
66. Jouvenot D, Koizumi M, Collin J-P, Sauvage J-P (2005) Eur J Inorg Chem, p 1850
67. Ballardini R, Balzani V, Gandolfi MT, Prodi L, Venturi M, Philp D, Ricketts HG, Stoddart JF (1993) Angew Chem Int Ed Eng 32:1301
68. Ashton PR, Ballardini R, Balzani V, Credi A, Dress KR, Ishow E, Kleverlaan CJ, Kocian O, Preece JA, Spencer N, Stoddart JF, Venturi M, Wenger S (2000) Chem Eur J 6:3558
69. Murakami H, Kawabuchi A, Kotoo K, Kunitake M, Nakashima N (1997) J Am Chem Soc 119:7605
70. Adelt M, Devenney M, Meyer TJ, Thompson DW, Treadway JA (1998) Inorg Chem 37:2616
71. Van Houten J, Watts J (1978) Inorg Chem 17:3381
72. Suen HF, Wilson SW, Pomerantz M, Walsch JL (1989) Inorg Chem 28:786
73. Pinnick DV, Durham B (1984) Inorg Chem 23:1440
74. Durham B, Caspar JV, Nagle JK, Meyer TJ (1982) J Am Chem Soc 104:4803
75. Tachiyashiki S, Mizumachi K (1994) Coord Chem Rev 132:113
76. von Zelewsky A, Gremaud G (1988) Helv Chim Acta 71:1108
77. Hichida H, Tachiyashiki S, Sasaki Y (1989) Chem Lett 1579
78. Collin J-P, Laemmel A-C, Sauvage J-P (2001) New J Chem 25:22
79. Baranoff E, Collin J-P, Furusho J, Furusho Y, Laemmel A-C, Sauvage J-P (2002) Inorg Chem 41:1215
80. Laemmel A-C, Collin J-P, Sauvage J-P, Accorsi G, Armaroli N (2003) Eur J Inorg Chem, p 467
81. Laemmel A-C, Collin J-P, Sauvage J-P (2000) CR Acad Sci 3:43
82. Bonnet S, Collin J-P, Gruber N, Sauvage J-P, Schofield ER (2003) Dalton Trans
83. Schofield ER, Collin J-P, Gruber N, Sauvage J-P (2003) Chem Commun, p 188
84. Bonnet S, Schofield ER, Collin J-P, Sauvage J-P (2004) Inorg Chem 43:8346
85. Sauvage J-P, Dietrich-Buchecker CO (eds) (1999) Molecular Catenanes, Rotaxanes and Knots. Wiley, Weinheim
86. Baranoff E, Collin J-P, Furusho Y, Laemmel A-C, Sauvage J-P (2000) Chem Commun, p 1935

87. Leising RA, Grzybowski J-J, Takeuchi KJ (1988) Inorg Chem 27:
88. Perez WJ, Lake CH, See RF, Toomey LM, Churchill MR, Takeuchi KJ, Radano CP, Boyko WJ, Bessel CA (1999) J Chem Soc Dalton Trans, p 2281
89. Cardenas DJ, Gavina P, Sauvage J-P (1997) J Am Chem Soc 119:2656
90. Fujita M (1999) Acc Chem Res 32:53
91. Hecker CR, Fanwick PE, McMillin DR (1991) Inorg Chem 30:659
92. Dudek MJ, Ponder JW (1995) J Comput Chem 16:791
93. Shinkai S, Nakaji T, Nishida Y, Ogawa T, Manabe O (1980) J Am Chem Soc 102:5860
94. Fabbrizzi L, Foti F, Patroni S, Pallavicini P, Taglietti A (2004) Angew Chem Int Ed Eng 43:5073
95. Pomeranc D, Jouvenot D, Chambron J-C, Collin J-P, Heitz V, Sauvage J-P (2003) Chem Eur J 9:4247
96. Balzani V, Credi A, Venturi M (1998) Coord Chem Rev 171:3
97. Hayoz P, von Zelewsky A, Stoeckli-Evans H (1993) J Am Chem Soc 115:51111
98. Arico F, Mobian P, Kern J-M, Sauvage J-P (2003) Organic Lett 5:1887
99. Mobian P, Kern J-M, Sauvage J-P (2003) J Am Chem Soc 125:2016
100. Mobian P, Kern J-M, Sauvage J-P (2003) Helv Chim Acta 86:4195